



**HAL**  
open science

# The Intra-Seasonal Oscillation of Precipitation $\delta^{18}\text{O}$ Over the Asian Equatorial and Monsoon Regions

Xuejie Wang, Lide Tian, Hongming Yan, Jiangyu Mao, Zhongyin Cai, Di  
Wang, Yiliang Cheng, Feng Liu

► **To cite this version:**

Xuejie Wang, Lide Tian, Hongming Yan, Jiangyu Mao, Zhongyin Cai, et al.. The Intra-Seasonal Oscillation of Precipitation  $\delta^{18}\text{O}$  Over the Asian Equatorial and Monsoon Regions. *Journal of Geophysical Research: Atmospheres*, 2023, 128, 10.1029/2023JD038869 . insu-04195508

**HAL Id: insu-04195508**

**<https://insu.hal.science/insu-04195508v1>**

Submitted on 7 Dec 2023

**HAL** is a multi-disciplinary open access archive for the deposit and dissemination of scientific research documents, whether they are published or not. The documents may come from teaching and research institutions in France or abroad, or from public or private research centers.

L'archive ouverte pluridisciplinaire **HAL**, est destinée au dépôt et à la diffusion de documents scientifiques de niveau recherche, publiés ou non, émanant des établissements d'enseignement et de recherche français ou étrangers, des laboratoires publics ou privés.

Copyright

# JGR Atmospheres

## RESEARCH ARTICLE

10.1029/2023JD038869

### Key Points:

- The intra-seasonal oscillations are one of the main patterns of precipitation  $\delta^{18}\text{O}$  covering the Asian monsoon and equatorial regions
- The stronger  $\delta^{18}\text{O}$  intra-seasonal oscillation corresponds to the season with active convective activities, more rainfall, and low-level  $\delta^{18}\text{O}$
- The stronger regional convective intensity leads to the cumulative effect in the depletion of rain  $\delta^{18}\text{O}$  during the convective phases of ISO

### Supporting Information:

Supporting Information may be found in the online version of this article.

### Correspondence to:

L. Tian,  
[ldtian@ynu.edu.cn](mailto:ldtian@ynu.edu.cn)

### Citation:

Wang, X., Tian, L., Yan, H., Mao, J., Cai, Z., Wang, D., et al. (2023). The intra-seasonal oscillation of precipitation  $\delta^{18}\text{O}$  over the Asian equatorial and monsoon regions. *Journal of Geophysical Research: Atmospheres*, 128, e2023JD038869. <https://doi.org/10.1029/2023JD038869>





Received 8 APR 2023

Accepted 11 JUN 2023

### Author Contributions:

**Conceptualization:** Xuejie Wang, Jiangyu Mao  
**Data curation:** Xuejie Wang, Yiliang Cheng, Feng Liu  
**Formal analysis:** Xuejie Wang, Di Wang  
**Funding acquisition:** Lide Tian  
**Investigation:** Xuejie Wang, Hongming Yan, Di Wang, Yiliang Cheng  
**Methodology:** Xuejie Wang, Lide Tian, Hongming Yan, Jiangyu Mao, Zhongyin Cai  
**Project Administration:** Lide Tian  
**Software:** Xuejie Wang  
**Supervision:** Lide Tian  
**Validation:** Xuejie Wang, Lide Tian, Zhongyin Cai  
**Visualization:** Xuejie Wang, Yiliang Cheng, Feng Liu

## The Intra-Seasonal Oscillation of Precipitation $\delta^{18}\text{O}$ Over the Asian Equatorial and Monsoon Regions

Xuejie Wang<sup>1,2</sup> , Lide Tian<sup>1,2</sup> , Hongming Yan<sup>3</sup>, Jiangyu Mao<sup>4</sup> , Zhongyin Cai<sup>1,2</sup> , Di Wang<sup>1,2,5</sup>, Yiliang Cheng<sup>1,2</sup>, and Feng Liu<sup>1,2</sup>

<sup>1</sup>Institute of International Rivers and Eco-security, Yunnan University, Southwest United Graduate School, Kunming, China, <sup>2</sup>Yunnan Key Laboratory of International Rivers and Transboundary Eco-security, Kunming, China, <sup>3</sup>Yunnan Climate Center, Yunnan Meteorological Administration, Kunming, China, <sup>4</sup>State Key Laboratory of Numerical Modeling for Atmospheric Sciences and Geophysical Fluid Dynamics (LASG), Institute of Atmospheric Physics, Chinese Academy of Sciences, Beijing, China, <sup>5</sup>Laboratoire de Météorologie Dynamique, IPSL, CNRS, Sorbonne Université Campus Pierre et Marie Curie, Paris, France

**Abstract** Water isotopes-climate correlations are used to reconstruct paleoclimate from various natural archives. Intra-seasonal oscillation is one of the major atmospheric patterns that modulate the ratio of precipitation isotope in low latitudes, yet their spatial and temporal distribution patterns are unclear. Here we presented a detailed analysis of how the intra-seasonal oscillations (MJO, Madden-Julian Oscillation, and BSISO, Boreal Summer Intra-seasonal Oscillation) modulate precipitation  $\delta^{18}\text{O}$  and vapor  $\delta^{18}\text{O}$  over the Asian monsoon region and the equatorial region. This analysis found consistent intra-seasonal variations between the ISO and rain  $\delta^{18}\text{O}$ . We interpret it as the ISO regulating the active and inactive convective systems on the regional scale, leading to the intra-seasonal oscillations in precipitation  $\delta^{18}\text{O}$ , with amplitudes from 4‰ up to 15‰. The MJO (BSISO) leads to eastward (northeastward) propagation of  $\delta^{18}\text{O}$  intra-seasonal oscillations in the Asian equatorial (monsoon) region, coinciding with the spatial patterns of OLR oscillations, reflecting the response of precipitation/vapor  $\delta^{18}\text{O}$  to the oscillation of large-scale convective activity or accumulated depletion of regional precipitation. We proved that the amplitudes of intra-seasonal variation of precipitation  $\delta^{18}\text{O}$  are comparable to seasonal variations, and both of them are the main patterns for precipitation  $\delta^{18}\text{O}$  in study regions. Our results are conducive to the accurate interpretation of  $\delta^{18}\text{O}$  in climate proxies such as precipitation, ice cores, tree cellulose, cave stalagmites, et al. on the intra-seasonal scale in this region.

**Plain Language Summary** Periodicity is a phenomenon in which similar characteristics or states of things reappear steadily and continuously. The Tropical Intra-seasonal Oscillation (Andersen et al., 2004, <https://doi.org/10.1038/nature02805>) is the reappearance of a large-scale envelope of more abundant convective rain systems moving eastward in the tropical regions with a typical oscillatory period of 30–60 days. The ratios of  $\text{H}_2^{18}\text{O}$  and HDO vary during the cycle of continuous circulation of water in the atmosphere, and therefore are widely used as proxies for climate records. We used the measured data of precipitation or vapor isotopes to reveal that the propagation of ISO can be recorded by the ratio of  $\text{H}_2^{18}\text{O}$  covering Asian tropical and monsoon regions. Furthermore, the increased (decreased) ISO intensity leads to the increased (decreased) amplitude of convection intensity, which results in the increased (decreased) amplitude of the  $\text{H}_2^{18}\text{O}$  ratio in precipitation or vapor.

## 1. Introduction

Understanding the spatiotemporal patterns of stable water isotopes in precipitation and vapor is important for the reconstruction of paleoclimate from various isotope archives, large-scale atmospheric circulation, hydrological cycles, and ecology studies. Specifically, unraveling the controls on stable isotopologues of tropical rainfall is critical for the extraction of paleoclimate information from tropical ice core (Permana et al., 2016; Thompson et al., 2000; Vimeux et al., 2005), stalagmite (Cheng et al., 2019; Murgulet & Aharon, 2008; Sinha et al., 2015; Tan et al., 2019; H. Zhang et al., 2018) and tree ring records (Islam et al., 2021; Liu et al., 2017; Ramesh et al., 1989). Yet, the interpretations of these isotope signals from archives are in the argument. The reconstruction of paleoclimate changes from Tibetan ice cores (Thompson et al., 1997) is challenged either by the inconsistency of the isotope record (Pang et al., 2020) or by the different interpretations of climate controls (Brown et al., 2006). Earlier studies focused on the local effects on precipitation isotopes, such as local air

**Writing – original draft:** Xuejie Wang, Lide Tian, Zhongyin Cai  
**Writing – review & editing:** Xuejie Wang, Di Wang

temperature and precipitation amount in the tropical and low-latitude regions (Araguás-Araguás et al., 1998; Dansgaard, 1964). However, more recent studies have emphasized the strong signal of large regional atmospheric circulation on precipitation isotopes (Lekshmy et al., 2014; Rahul et al., 2016; D. Wang et al., 2020), for example, the ENSO signal in precipitation (Cai et al., 2017; Vuille & Werner, 2005; H. Yang et al., 2016), ice core record (Shao et al., 2017; X. Yang, Yao, et al., 2018) and tree ring as well (Liu et al., 2017). The signal of atmospheric circulation is probably holding for an even longer time scale in ice core isotope records (Porter et al., 2021).

The spatial and temporal patterns of precipitation  $\delta^{18}\text{O}$  on seasonal and inter-annual scales covering the Asian monsoon and tropical regions have been discussed in recent years. Seasonally, the sharp drop in precipitation  $\delta^{18}\text{O}$  in the early summer in monsoonal Asia is related to the atmospheric circulation pattern with the strong monsoon convection precipitation, the high cloud top and the low condensation temperature (Cai & Tian, 2016) corresponding to the summer monsoon onset and northward migration of the Intertropical Convergence Zone (ITCZ) (Cai et al., 2018; X. Yang et al., 2012). On the inter-annual scale, the precipitation  $\delta$ -value contains information about the El Niño–Southern Oscillation and the Intertropical Convergence Zone in the Asian tropical region (He, Goodkin, Jackisch, et al., 2018), and in association with the East Asian summer and winter monsoon intensity in the monsoon region (Kurita et al., 2015). On the large spatial scales, the positive CTP (cloud top pressure) anomalies in the central Indo-Pacific within the weak Walker circulation (El Niño) are associated with positive  $\delta^{18}\text{O}$  anomalies (Cai & Tian, 2016). How the pattern of precipitation isotope is influenced by intra-seasonal oscillations (Andersen et al., 2004) should also be addressed, as the ISO is the major pattern to modulate the level of convective activity in the low latitude region on the intra-seasonal time scale. The underlying processes resulting in isotopic fractionation during the aforementioned time scales are based on the Rayleigh processes (Dansgaard, 1964) under the equilibrium and based on the kinetic fractionation from evaporation to precipitation.

The intra-seasonal oscillations (Andersen et al., 2004) have two patterns: the Madden-Julian Oscillation (MJO, during the DJFMA) (Madden & Julian, 1972) and the Boreal Summer Intra-seasonal Oscillation (BSISO, during the JJASO) (Kikuchi, 2021). MJO consists of large-scale coupled patterns in atmospheric circulation and deep convection (C. Zhang, 2005), which can affect precipitation on a global scale and serve as a prominent source of monsoon intra-seasonal fluctuations (Donald et al., 2006; C. Zhang, 2013). BSISO displays a more complicated spatiotemporal evolution than MJO, characterized by northward propagation over the northern Indian Ocean and western North Pacific as well as eastward propagation along the equator during boreal summer (Goswami & Mohan, 2001; Sperber et al., 2000). The ISO also has a wide range of low-frequency and low-pressure convective oscillations superimposed on the Intertropical Convergence Zone (ITCZ) (Jiang et al., 2020; T. Li, 2014), and has the widest coverage and highest amplitude between Asia and Australia. Considering those features, the ISO may exert its influence on stable isotopes in vapor or precipitation in a wide region by modulating convective activity on the propagation path eastward and poleward.

Earlier studies have revealed that the  $^{18}\text{O}$  depletion in monsoon rain is related to large-scale organized convection (Lekshmy et al., 2014) and appeared to be linked with the monsoon intra-seasonal variability or oscillation in addition to synoptic scale fluctuations (Chakraborty et al., 2016; Risi et al., 2008; Sengupta et al., 2020). It is reported that the Indian summer monsoon rainfall  $\delta^{18}\text{O}$  of southwestern India captures not only the local or upstream convective activities but reflects the rainfall pattern of a large domain (Lekshmy et al., 2019). The dilution of rainfall  $\delta^{18}\text{O}$  accompanying the increased proportion of large-scale stratiform cloud cover of the deep convective system during the MJO onset period (Kurita et al., 2011). The isotopic variation in precipitation and variability in monsoon conditions, associated with the presence of large convective envelopes propagating through the north Australia on intra-seasonal or longer timescales (Zwart et al., 2016). These earlier findings allow for a further discussion of the intra-seasonal pattern of precipitation or vapor isotopes comprehensively over the southern Asian monsoon and equatorial regions.

This paper aims to address how the ISO is linked with the frequency and intensity of the intra-seasonal oscillation in precipitation and vapor  $\delta^{18}\text{O}$  across the Asian equatorial region and monsoon region, with an emphasis on the spatial coherence and variability of the two regions. Also, we will discuss their spatial impact on the water isotopes and the possible underlying mechanism with the MJO and BSISO propagation, together with the spatial and intra-seasonal oscillations of outgoing longwave radiation (OLR), precipitation, vapor flux, and convective system events. As the major  $\delta^{18}\text{O}$  pattern of tropical regions, the reveal of  $\delta^{18}\text{O}$  intra-seasonal oscillation is one of the research results for the Coordinated Research Project of the IAEA (International Atomic Energy Agency), Stable Isotopes in Precipitation and Paleoclimatic Archives in Tropical Areas to Improve Regional Hydrological and Climatic Impact Models (<https://www.iaea.org/projects/crpf31004>).

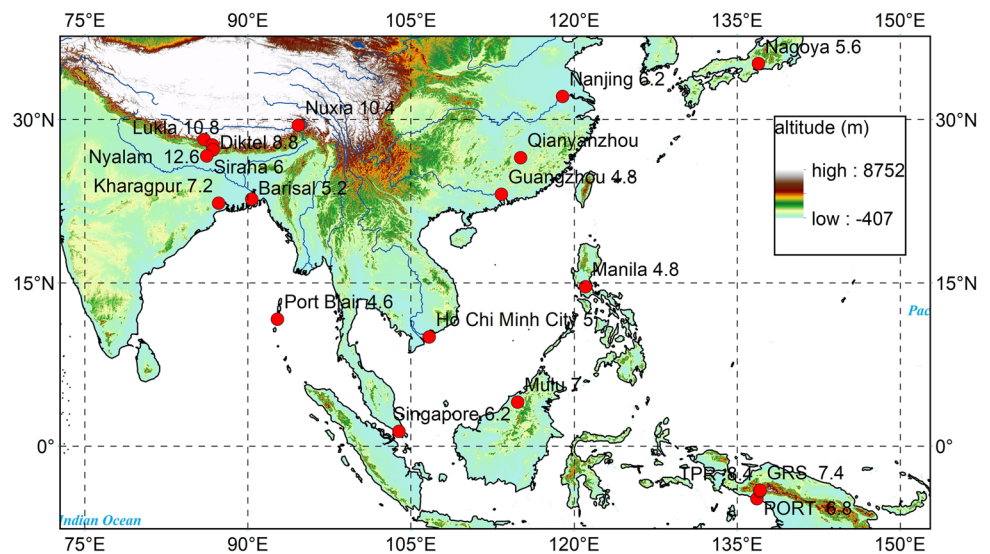


**Figure 1.** The geographical location of stations (marked in solid red dots). The number after the site name represents the amplitude threshold (twice the standard deviation,  $2\sigma$ ) of the intra-seasonal oscillation of precipitation  $\delta^{18}\text{O}$  (‰) at each site during the study period.

## 2. Data and Methods

### 2.1. The Geographical Location

The study region includes the southern part of the Asian monsoon and the equatorial region (the Maritime Continent) (Figure 1). The average annual precipitation is generally over 800 mm, with seasonality influenced by the summer monsoon and ITCZ. We used the daily measured  $\delta^{18}\text{O}$  data from 18 precipitation stations and one near-ground vapor station (Table S1 in Supporting Information S1). Stations in the monsoon region are affected by the BSISO, while stations in the equatorial region can be affected by both the MJO and BSISO.

### 2.2. Precipitation and Vapor Stable Isotope Data

In the equatorial region, we used the precipitation isotope data of Singapore, Mulu, PORT (Port site), TPR (Tembagapura), and GRS (Grasberg). In the South Asia monsoon region, the precipitation isotope measurement sites we used are Port Blair, Kharagpur, Barisal, Siraha, Diktel, Lukla, Nyalam, and Nuxia. In the Southeast Asia monsoon region, the precipitation isotope data of Ho Chi Minh City and Manila are used in this paper. In the East Asia monsoon region, we used the precipitation isotope data of Guangzhou, Nanjing, Nagoya, and the vapor isotope data of Qianyanzhou. Except for the data periods of PORT, TPR, and GRS, which are for 2013 and 2015, the data of other stations are for 2014.

In addition, the data from IASI (Infrared Atmospheric Sounding Interferometer) is used to provide grid data of  $\delta\text{D}$ , specific humidity, and air temperature of three cloud-free layers in the troposphere with a spatial resolution of  $1^\circ \times 1^\circ$  by scanning the globe twice every morning and evening starting from October 2014 (Diekmann et al., 2021).

### 2.3. Meteorological Data

The interpolated outgoing longwave radiation (OLR) data with a spatial resolution of  $2.5^\circ \times 2.5^\circ$  are used for the proxy index of convective intensity. The daily reanalysis climate data ( $u$  wind,  $v$  wind, and specific humidity) of ERA5 with a spatial resolution of  $0.25^\circ \times 0.25^\circ$  are used for the analysis of meteorological background field. The phases and indexes PCx or PCy of BSISO and MJO (Wheeler & Hendon, 2004) are represented the cycle and intensity of ISO. The EEOF coefficients (principal components, PCx or PCy) of the MJO or BSISO mode at any given time can be obtained by projecting the intra-seasonal time-filtered OLR fields onto each mode (Kikuchi et al., 2012). In addition, we used the typhoon track and intensity data in the northwest Pacific Ocean and precipitation data GPCP ( $1^\circ \times 1^\circ$ ), the latter is used to calculate the regional precipitation.



## 2.4. Methods

The criteria for defining significant intra-seasonal oscillations of  $\delta^{18}\text{O}$  and OLR are determined from their respective means ( $\mu$ ) and one standard deviation ( $1\sigma$ ) (beyond the range of  $\mu \pm 1\sigma$ ) (Lekshmy et al., 2019). The PCx or PCy index is used for judging the intensity of BSISO or MJO. We perform the student's-*t* test to determine whether the two mean values of precipitation  $\delta^{18}\text{O}$  are statistically different or not under the 0.05 significance level. The lead-lag correlation between two station  $\delta^{18}\text{O}$  series is used to diagnose the strength of spatial and temporal coherence quantitatively.

To analyze the periodic spectra of MJO and BSISO, we use the 10–80 days band-pass filtering function, `bw_bandpass_filter` (the Butterworth bandpass filter), of NCL software ([https://www.ncl.ucar.edu/Document/Functions/Built-in/bw\\_bandpass\\_filter.shtml](https://www.ncl.ucar.edu/Document/Functions/Built-in/bw_bandpass_filter.shtml)), to draw the spatiotemporal band-pass filtering features of the OLR anomaly over the study region. The purpose of bandpass filtering on OLR is to highlight the OLR anomaly signals on the intra-seasonal time scale (Sengupta et al., 2020). We used the daily wind field at 850 hPa (ERA5 data) to identify the Indian summer monsoon system. When the streamline of the wind field has a circular distribution in the Bay of Bengal and surrounding land, we can judge the formation of a monsoon depression.

To attenuate the high-frequency fluctuations of  $\delta^{18}\text{O}$  caused by synoptic-scale fluctuations and highlight the intra-seasonal scale variations, we made a 9-day running average process for the daily  $\delta^{18}\text{O}$  data of all stations. In this paper, the amplitude of each separate oscillation is calculated by the difference between the average values of the two shoulders of the oscillation curve and the trough value, and the amplitude of the intra-seasonal oscillations over the whole study period is defined as  $\mu \pm 1\sigma$ .

## 3. Results

### 3.1. Influence of the MJO and BSISO on Precipitation $\delta^{18}\text{O}$ Across the Equatorial Asian Stations

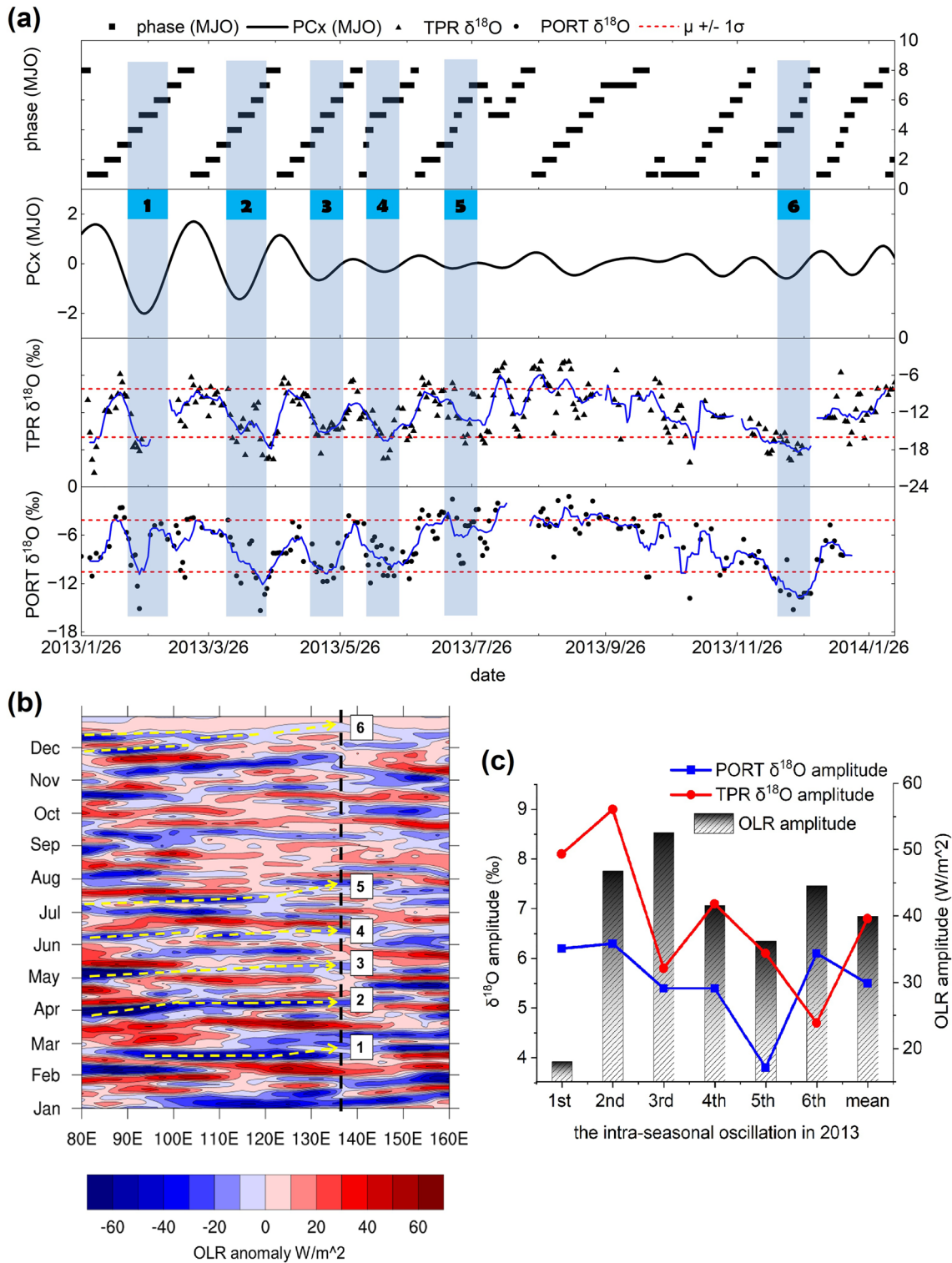
The convective systems of the ISO propagate eastward and poleward from the equatorial region both in the boreal winter and summer seasons (T. Li, 2014). Intra-seasonal rainfall  $\delta^{18}\text{O}$  variability, which is particularly large at northern Borneo with up to 16‰, is closely associated with the MJO, the dominant mode of intra-seasonal climatic variability in the tropics during winter, and exhibits influences of both local and regional atmospheric fractionation processes (Moerman et al., 2013). Here we first performed an analysis of the intra-seasonal variations of precipitation  $\delta^{18}\text{O}$  influenced by the MJO activities at two stations located in the equatorial Asia region.

Figure 2a shows the daily (scatter) and 9-day running average (blue curve) precipitation  $\delta^{18}\text{O}$  at the two stations (PORT and TPR) in eastern Indonesia combined with the phases and PCx index of MJO during 2013. Six distinct intra-seasonal oscillations of precipitation  $\delta^{18}\text{O}$  are identified from the two stations (the trough of the  $\delta^{18}\text{O}$  oscillation is marked in vertical shadows). Except for the fifth oscillation at PORT, the vibrations of  $\delta^{18}\text{O}$  at all the other five dilution processes are over one standard deviation.

The oscillation of precipitation  $\delta^{18}\text{O}$  at the two stations is roughly in phase with each other as they are close in distance (85 km) with the same longitude but a large altitude contrast (9 m a.s.l. and 1,900 m a.s.l.). The phases of the MJO are also presented in the picture as a comparison with the precipitation  $\delta^{18}\text{O}$  oscillations. The one standard deviations of  $\delta^{18}\text{O}$  in PORT and TPR are 3.2‰ and 3.9‰ respectively (Figure 2a), and the amplitude of precipitation  $\delta^{18}\text{O}$  variations during the active phase of the MJO is from 3.8‰ to 6.3‰ (PORT) and 4.7‰ to 9‰ (TPR) (Figure 2c) respectively.

The six precipitation  $\delta^{18}\text{O}$  oscillations correspond to the six cycles of the MJO phase (panel 1 in Figure 2a). The low periods of  $\delta^{18}\text{O}$  intra-seasonal oscillations appear in phases 4, 5, and 6 of the MJO, as the central convective region moved from the Maritime Continent to the Western Pacific (Table S2 and Figure S1 in Supporting Information S1), corresponding to the convective patterns covering the Indonesian archipelago (the trough period of PCx of the MJO).

With the influence of the movement of the ITCZ and the fact that two stations are located in the southern equatorial belt, the precipitation  $\delta^{18}\text{O}$  at the two stations is roughly at higher levels (with averages of  $-4.8\text{‰}$  and  $-8.5\text{‰}$ ) without significant intra-seasonal oscillation from July to October 2013. The six significant intra-seasonal oscillations appear in the lower precipitation  $\delta^{18}\text{O}$  (with averages of  $-8.5\text{‰}$  and  $-13.3\text{‰}$ ) during the other months of 2013 (Figure 2a), corresponding to the obvious influence of the OLR anomaly oscillation zone (Figure 2b). Figure 2b shows the temporal variations of the band OLR anomaly between  $10^{\circ}\text{S}$  and  $0^{\circ}\text{S}$  in the equatorial region



**Figure 2.** The daily (scatter) and 9-day running average (blue curve)  $\delta^{18}\text{O}$  at two equatorial stations (PORT and TPR) in eastern Indonesia compared with the phase and PCx of Madden-Julian Oscillation during 2013 (a). The shaded column marked by the numbers 1–6 indicates the six times of  $\delta^{18}\text{O}$  intra-seasonal oscillations at two stations; the horizontal red dashed pair lines show the range of data within  $\mu \pm 1\sigma$  (band  $-4.1\text{‰}$ – $-10.5\text{‰}$  for PORT and  $-8.2\text{‰}$ – $-16.0\text{‰}$  for TPR). The average outgoing longwave radiation (OLR) anomaly from  $10^\circ\text{S}$  to the equator, processed by band-pass filtering in 10–80 days (Hovmöller diagram) during 2013 (shaded, in  $\text{W/m}^2$ ), with the vertical black dashed line marking the longitude of the two stations (b). The six intra-seasonal oscillation amplitudes of OLR and precipitation  $\delta^{18}\text{O}$  at PORT and TPR during 2013 (c).

of Asia. The six lower precipitation  $\delta^{18}\text{O}$  events are in periods with lower OLR anomalies, the sign of strong convective systems. This occurrence indicates the lower precipitation isotope ratios at the two equatorial stations are associated with the propagation of the convective system belts from west to east in the intra-seasonal oscillations. We compared the amplitude of precipitation  $\delta^{18}\text{O}$  and OLR in the six oscillation events (Figure 2c) and see that the average local grid OLR oscillation is  $40 \text{ W/m}^2$ , corresponding to the average  $\delta^{18}\text{O}$  oscillations of  $5.5\text{‰}$  and  $6.8\text{‰}$  for TPR and PORT, respectively. We noticed that the 1st and 2nd oscillation events have lower OLR amplitude than the 3rd event, while the  $\delta^{18}\text{O}$  fluctuation in the 3rd event is larger than the former two. The likely reason is that there exists a strong persistent convection zone (blue band in Figure 2b) in the upper stream region of the station during the 1st and 2nd events, while the persistent negative OLR anomaly is less strong during the 3rd event.

As the seasonal north-south movement of the ITCZ can influence the intra-seasonal oscillation pattern of precipitation isotopes, following we will discuss the intra-seasonal oscillation of precipitation  $\delta^{18}\text{O}$  at Mulu station on the northern side of the equator.

There are nine complete ISO phase cycles (both BSISO and MJO modes) from 26 January 2013 to 7 February 2014 (Figure 3), accompanied by 11 oscillations of precipitation  $\delta^{18}\text{O}$  and eight dilution processes of precipitation  $\delta^{18}\text{O}$  exceeding one standard deviation. The 5th and 6th, 8th and 9th  $\delta^{18}\text{O}$  oscillations occurred in two longer period cycles of ISO activity (57 and 49 days, respectively). The lower precipitation  $\delta^{18}\text{O}$  periods within the intra-seasonal oscillation usually occur at phases 2, 3, 4, and 5 of ISO, one phase (5 days approximately) ahead of the PORT and TPR sites (Figure 2a). All the 11  $\delta^{18}\text{O}$  oscillation events correspond to the fluctuations of OLR anomaly bands propagating to the Mulu site (Figure 3b).

Compared with TPR and PORT stations, the significant intra-seasonal oscillation of precipitation  $\delta^{18}\text{O}$  to the north of the equator is found throughout the whole year without obvious seasonal differences (Figure 3a). To quantitatively explore the influence of the oscillation intensity of ISO on the precipitation  $\delta^{18}\text{O}$ , we made correlation scatter graphs between  $\delta^{18}\text{O}$  and the PCx of two ISO modes (Figure 3c). Significant positive correlations are found between PCx of BSISO and  $\delta^{18}\text{O}$ , indicating that both the BSISO and MJO can significantly affect the intra-seasonal oscillation of precipitation isotopes (with large magnitudes from  $-3.9\text{‰}$  to  $-11.7\text{‰}$ ) in that region throughout the year.

### 3.2. The Pattern of Precipitation and Vapor $\delta^{18}\text{O}$ Affected by the Propagation of BSISO at the Asian Monsoon Stations

#### 3.2.1. The Overview of Precipitation/Vapor $\delta^{18}\text{O}$ Oscillation Across the Stations

The BSISO is predominant in the JJASO, whereas the MJO is in the DJFMA, while May and November are transitional months (Kikuchi, 2021; Kikuchi et al., 2012). Therefore, we study the intra-seasonal variation of precipitation and vapor  $\delta^{18}\text{O}$  as a response to BSISO propagation from May to October. Here, we include May as the onset month of the Asian summer monsoon.

We plot the graphs showing the temporal variations of daily precipitation and vapor  $\delta^{18}\text{O}$  at five stations in southern Asia together with the cycles of BSISO as a comparison (Figure 4). The five stations have relatively scattered spatial distribution for the purpose to show the overall characteristics of precipitation  $\delta^{18}\text{O}$  intra-seasonal oscillations in the study regions. From May to October 2014, the six BSISO events were roughly in phase with the precipitation  $\delta^{18}\text{O}$  oscillations. The slight phase difference in precipitation  $\delta^{18}\text{O}$  is related to the locations of these stations and the propagation of BSISO from south to north. From phases 1 to 8 of the BSISO, the central convective region propagate across the equatorial Indian Ocean, the Bay of Bengal, the Indian & Maritime continent, the Western North Pacific, and lastly to the Eastern North Pacific Ocean (Table S2 in Supporting Information S1) (Kikuchi et al., 2012). The convective band of the BSISO spread from the southwest to the northeast in the Asian monsoon region (Figure S1 in Supporting Information S1). In addition, the fluctuation of the convective band with northwest-southeast trending is presented, which respectively corresponds to the activity of monsoon depressions (Goswami, 1987; Goswami et al., 2003), monsoon cloud clusters and tropical cyclones (Figure S2 in Supporting Information S1) from the Indian subcontinent to the northwest Pacific Ocean via Indochina Peninsula. The rainfall/vapor isotopes show signatures of monsoon depressions, which has been presented in previous studies (Midhun et al., 2013, 2018). The phase of the  $\delta^{18}\text{O}$  negative anomaly in the northern station (Qianyanzhou) lagged the southern station (Singapore) (Figure 4). In the fifth oscillation as shown in Figure 4a, the arrival date and the trough value of  $\delta^{18}\text{O}$  oscillation at each station are Singapore (29 August,  $-11.3\text{‰}$ ), Nyalam (11 September,  $-18.5\text{‰}$ ), Guangzhou (11 September,  $-9.3\text{‰}$ ), and Qianyanzhou (18 September,  $-17.3\text{‰}$ ). As the

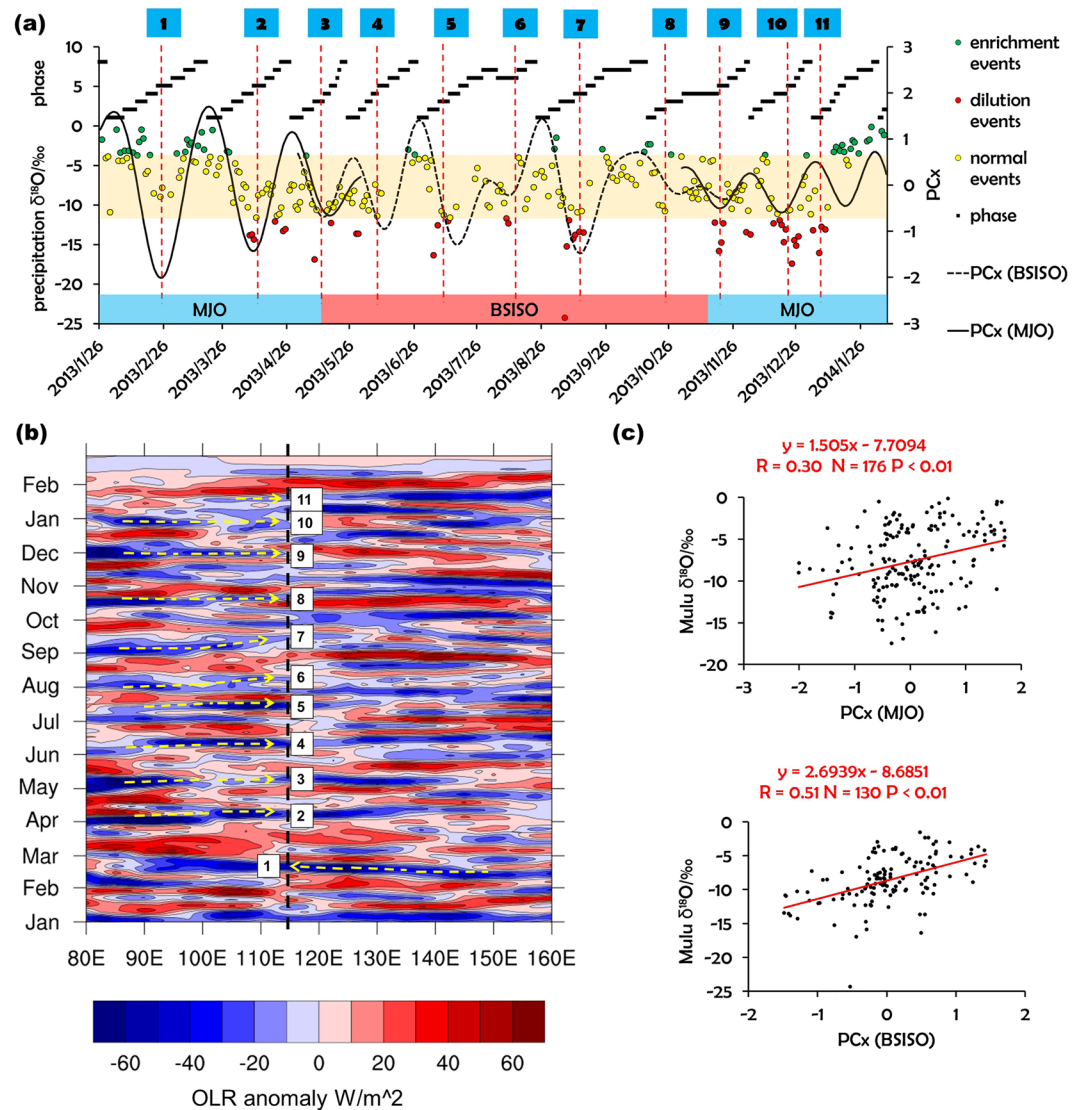


**Figure 3.** The daily (scatter)  $\delta^{18}\text{O}$  at Mulu, Eastern Malaysia, compared with the phase and PCx cycles of Madden-Julian Oscillation (MJO) and Boreal Summer Intra-seasonal Oscillation (BSISO) during 2013 (a), the orange envelope showing the range of data within  $\mu \pm 1\sigma$  (band  $-3.9\text{‰}$ – $-11.7\text{‰}$ ), the top numbers 1–11, and the vertical red dashed line marking the depleted phase of Mulu  $\delta^{18}\text{O}$ . The average outgoing longwave radiation (OLR) anomaly from the equator to  $10^\circ\text{N}$ , processed by band-pass filtering in 10–80 days (Hovmöller diagram) from January 2013 to February 2014 (shaded, in  $\text{W}/\text{m}^2$ ), the vertical black dashed line marking the longitude of the Mulu station (b), the blue band marking numbers 1–11 with yellow slanted dashed arrows showing the propagation of convective activities (negative OLR anomaly), matching the depleted phase of Mulu  $\delta^{18}\text{O}$  marked numbers. The two scatter plots show the Mulu precipitation  $\delta^{18}\text{O}$  versus PCx of MJO (during NDJFMAM) and PCx of BSISO (during MJJASON) (c).

convective phase of BSISO propagated from Singapore to Qianyanzhou, precipitation or vapor  $\delta^{18}\text{O}$  fluctuated in phase with the oscillation of OLR, and the propagation duration was about 20 days. The BSISO exerts regulation effect on the frequency and intensity of convective systems both in South Asia and East Asia when the convective phase is present. Although these precipitation or vapor  $\delta^{18}\text{O}$  between two stations (such as Nyalam and Qianyanzhou) are not affected by the same convective system, they are regulated by the same one BSISO cycle.

### 3.2.2. Precipitation/Vapor $\delta^{18}\text{O}$ Variation With the Propagation of the BSISO Along the Four Spatial Transects

As the pattern of tropical ISO propagates both northward and eastward in the boreal summer in association with OLR (S. Wang et al., 2018), here we provide an approach to diagnose how precipitation  $\delta^{18}\text{O}$  responds to the



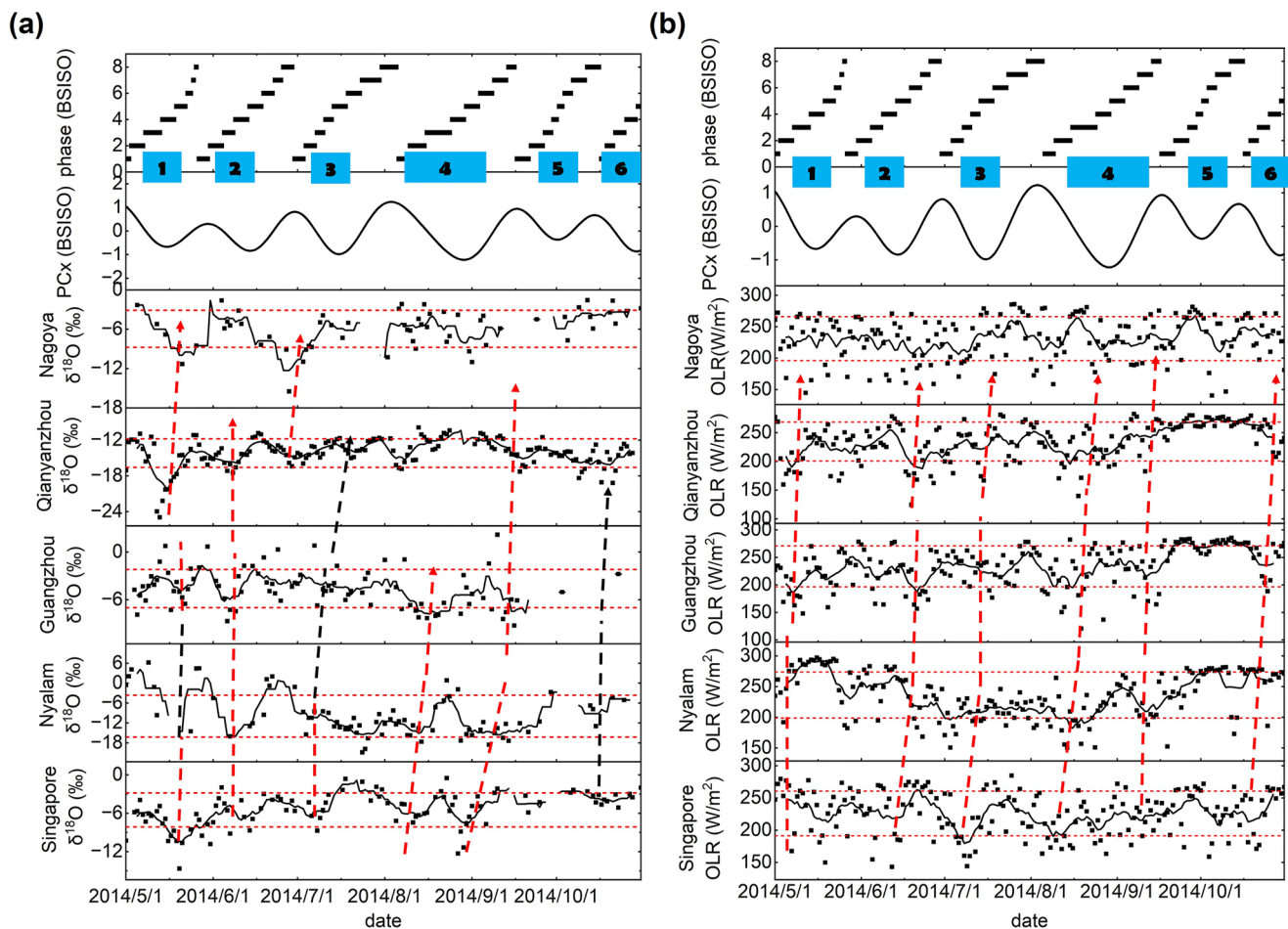


**Figure 4.** The daily (scatter) and 9-day running average precipitation  $\delta^{18}\text{O}$  (a) and the outgoing longwave radiation (OLR) value (b) at Singapore, Nyalam, Guangzhou, Nagoya, and Qianyanzhou (vapor  $\delta^{18}\text{O}$ ), and the phase of Boreal Summer Intra-seasonal Oscillation (BSISO) from May to October 2014. The slanted dashed lines with arrows are low-value phases of precipitation  $\delta^{18}\text{O}$  and OLR concerning the BSISO propagation events (the red line represented the precipitation  $\delta^{18}\text{O}$  reaching the  $1\sigma$  level). The short horizontal dashed lines represent the  $\mu \pm 1\sigma$  level of  $\delta^{18}\text{O}$  and OLR at each station. The lag of phase in both precipitation  $\delta^{18}\text{O}$  and OLR reflects the BSISO propagation from the equatorial region to the northern monsoon region.

BSISO phase change spatially and temporally by analyzing the coherent oscillations of rainfall or near-ground vapor isotope along four profiles.

Profile 1 represents the south-north propagation of BSISO from the Bay of Bengal to the southern Tibetan Plateau, and here we have precipitation  $\delta^{18}\text{O}$  oscillations at four stations: Port Blair, Barisal, Nyalam, and Nuxia.

We can identify six precipitation  $\delta^{18}\text{O}$  depletion events from those seasonal  $\delta^{18}\text{O}$  series at the four stations (Figure 5a), roughly coherent with the six occurrences of negative OLR anomaly bands in Figure 6a. We see a gradual propagation of the negative OLR anomaly belt from the equatorial region to around  $30^\circ\text{N}$  with a lag of a couple of days, leading to a slight mismatch in the phase change of precipitation  $\delta^{18}\text{O}$  at the four stations. The responses of the intra-seasonal oscillation of precipitation  $\delta^{18}\text{O}$  differ in their variation magnitude at the four stations. Nyalam and Nuxia have significant negative average precipitation  $\delta^{18}\text{O}$  ( $-9.9\text{‰}$  and  $-9.3\text{‰}$ ) compared with Barisal and Port Blair ( $-4.5\text{‰}$  and  $-3.0\text{‰}$ ) from May to October 2014 (under the student's  $t$  test at 0.05 levels, Tables S3 and S4 in Supporting Information S1). The amplitude of the precipitation  $\delta^{18}\text{O}$  oscillation at the two southern stations (Port Blair and Barisal) is less pronounced about  $5\text{‰}$  (Figure 5a; Table S3 in Supporting Information S1). But the northern stations (Nyalam and Nuxia) on the southern slope of the Himalaya have the higher and more pronounced precipitation  $\delta^{18}\text{O}$  amplitude of about  $10\text{‰}$ . We also found a phenomenon that the two oceanic stations have the largest OLR oscillation while having the least precipitation  $\delta^{18}\text{O}$  fluctuations. Whereas the two plateau stations have the least OLR oscillation but larger intra-seasonal  $\delta^{18}\text{O}$  fluctuations. We explain this as the weak fractionation during the initial stage of Rayleigh distillation in the moisture source region for the tropical stations, which can be supported by the higher precipitation



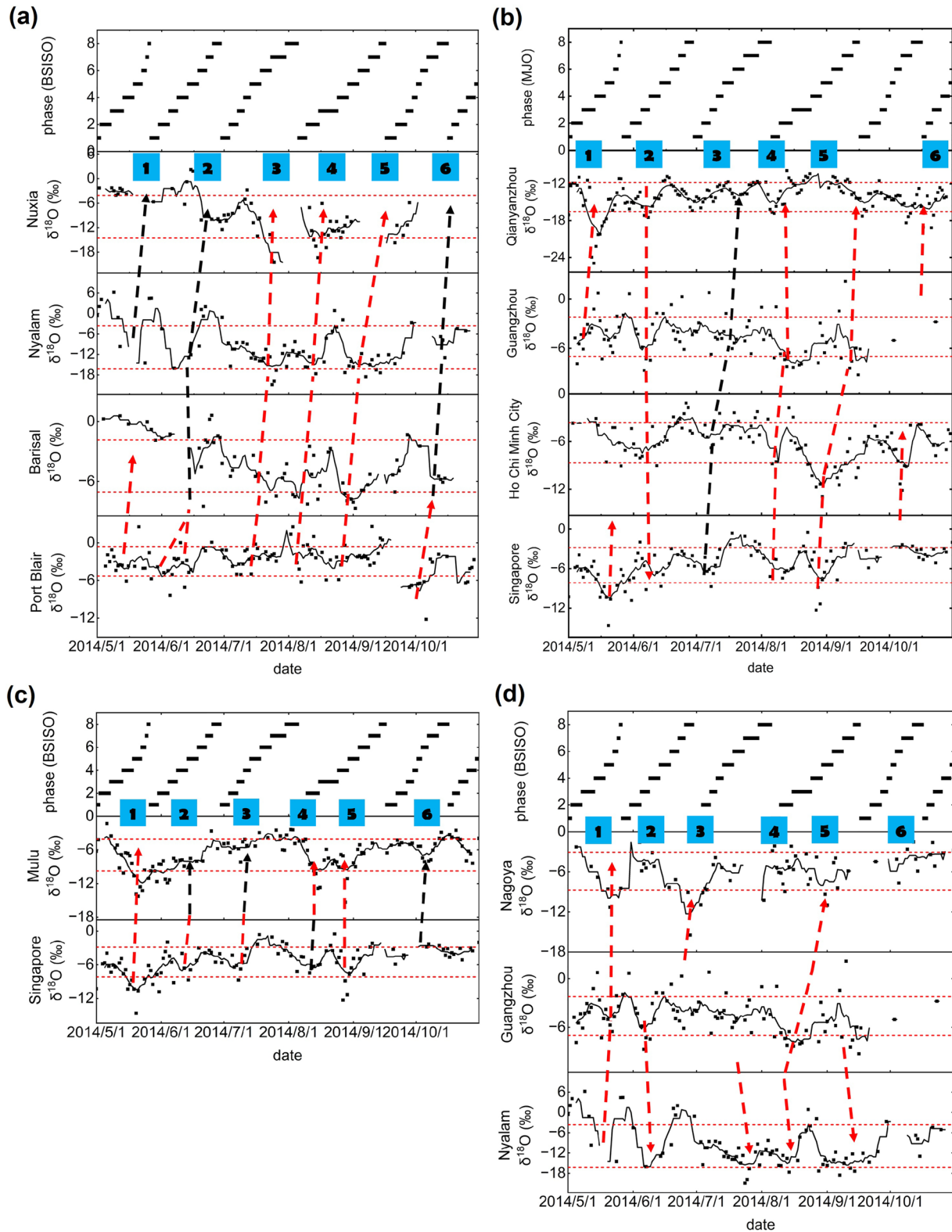


**Figure 5.** The daily and 9-day running average of precipitation  $\delta^{18}\text{O}$  at the stations from May to October 2014 along profiles 1 (a), 2 (b), 3 (c), and 4 (d). The red or black slanted dashed lines with arrows and corresponding numbers indicate the low-value phases of  $\delta^{18}\text{O}$  reach or do not reach the threshold of one standard deviation. The short horizontal dashed lines represent the  $\mu \pm 1\sigma$  level of  $\delta^{18}\text{O}$  and outgoing longwave radiation at each station.

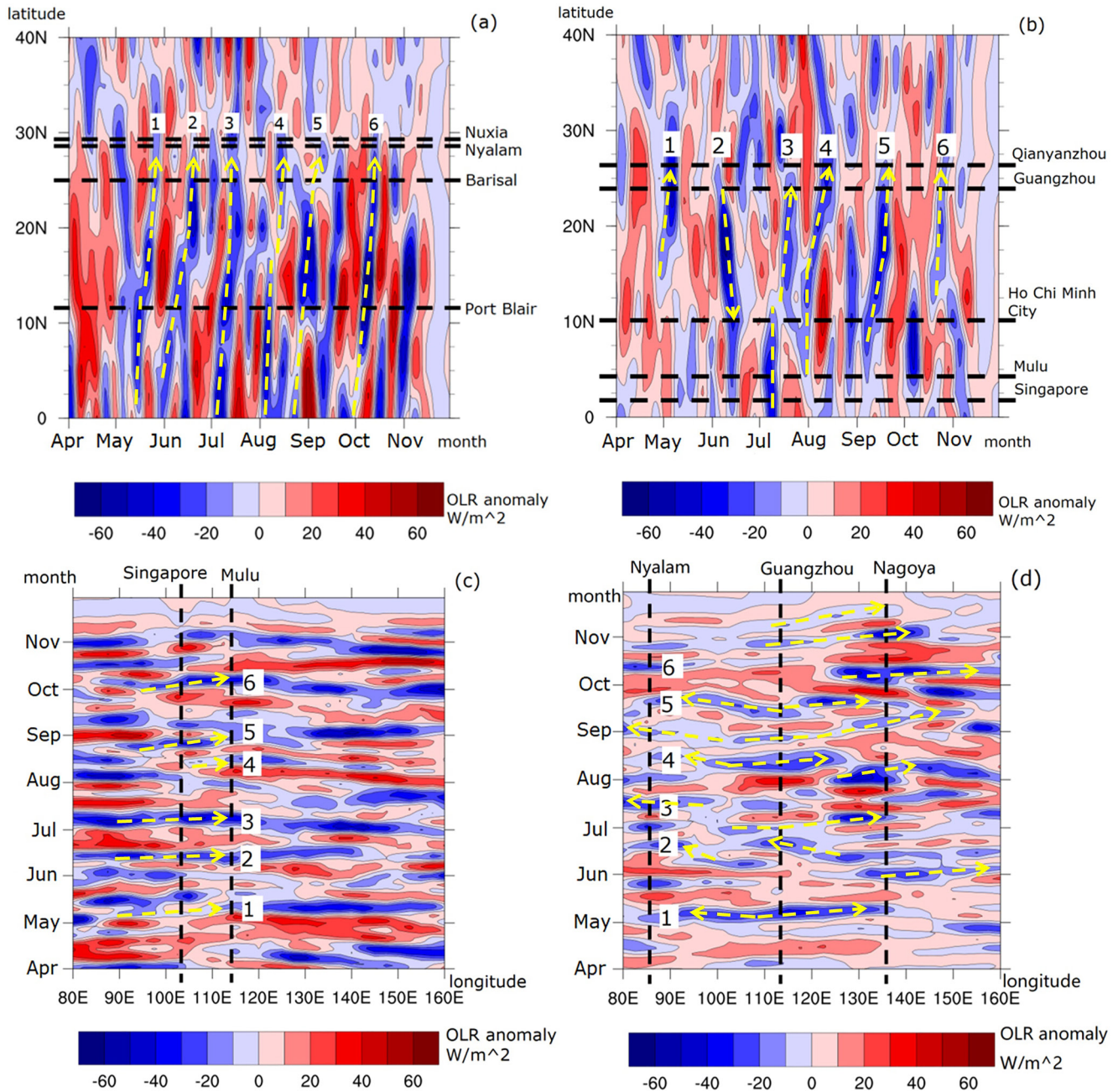


**Figure 6.** Longitude average (80°E–95°E, (a)); 100°E–120°E, (b)) time–latitude representation (Hovmöller plot) and latitude average (0°–10°N, (c); 20°N–35°N, (d)) longitude–time representation (Hovmöller plot) of 10–80 days of filtered outgoing longwave radiation (OLR) anomaly (shaded, W/m<sup>2</sup>) during 2014. The blue band marked numbers with yellow slanted dashed arrows show the propagation of convective activities (negative OLR anomaly), matching the low level of  $\delta^{18}\text{O}$  marked numbers in Figure 5. The horizontal or vertical black dashed lines represent the latitude or longitude of the stations.

$\delta^{18}\text{O}$  at the two stations (from positive to about  $-8\text{‰}$ ) and more depleted precipitation  $\delta^{18}\text{O}$  from over  $0\text{‰}$  to as low as  $-16\text{‰}$  at the two plateau stations. Quite a few recent works confirmed that the precipitation isotope is a combined effect of the on-route rainout fractionation on the southern Tibetan Plateau. In particular, the strong convection precipitation in the upstream region of the southern Tibetan Plateau produced extremely depleted water isotopes (Cai et al., 2018; Dong et al., 2016). This effect enlarges the intra-seasonal oscillation signal in the later precipitation.

Profile 2 is another south–north propagation of BSISO along the Central Indonesia Archipelago, the East Indochina Peninsula, and the South China Sea to South China. Here we have four stations with precipitation/vapor  $\delta^{18}\text{O}$  data in this profile: Singapore, Ho Chi Minh City, Guangzhou, and Qianyanzhou.

Figures 5b and 6b are the temporal variations of  $\delta^{18}\text{O}$  at the four stations in 2014 and the time-latitude diagram of the OLR anomaly. Three of those stations (Singapore, Ho Chi Minh City, and Guangzhou) have a similar range of precipitation  $\delta^{18}\text{O}$  of roughly between  $-2\text{‰}$  and  $-8\text{‰}$ . Qianyanzhou, the most northern and inland vapor station, has depleted vapor  $\delta^{18}\text{O}$  within  $-12\text{‰}$  to  $-20\text{‰}$ . We can identify six strong continuous north-south negative OLR anomaly bands from June to September, and the amplitude of the OLR oscillation could be as high as about  $70\text{ W/m}^2$ , corresponding to the oscillations of precipitation or vapor  $\delta^{18}\text{O}$  in the range of about  $6\text{‰}$ .

Profile 3 is a west-to-east propagation path of the BSISO near the equatorial belt with two stations, Singapore and Mulu. Most of the precipitation  $\delta^{18}\text{O}$  values at the two stations are in the range from  $-2\text{‰}$  to  $-10\text{‰}$  (Figure 5c). There are six low  $\delta^{18}\text{O}$  bands with strong synchronization between the two stations, and the amplitude of each oscillation is significantly consistent due to the relatively short distance (Figure 5c). Figure 6c shows the temporal propagation of the filtered OLR anomaly in the latitude zone from  $0^\circ$  to  $10^\circ\text{N}$ . The six negative OLR bands at the two stations are in strong east-west continuity and are synchronous with the six lower  $\delta^{18}\text{O}$  events, as shown in Figure 5c.

Figures 5c and 6c also show that BSISO has fluctuations in both frequency and strength in the equatorial region. However, we also found that the larger coherent depletion of precipitation  $\delta^{18}\text{O}$  at the two stations as in events 1, 4, and 5 (Figure 5c) has no corresponding agreement in the lower OLR cells (Figure 6c).

Profile 4 is another west-east belt at  $20^\circ\text{N}$ – $35^\circ\text{N}$  in the Asian monsoon region. There are three stations along this profile: Nyalam, Guangzhou, and Nagoya. The continuity of the negative OLR cells is interrupted by the frequent higher OLR cells (Figure 6d), as compared with profile 3 (Figure 6c). There are three negative OLR cell centers roughly surrounding the meridian of the three stations (Figure 6d). The discontinuity and isolation of the negative OLR cells probably produced poor coherence variations with the precipitation  $\delta^{18}\text{O}$  oscillations at the three stations. The east two stations show weaker  $\delta^{18}\text{O}$  intra-seasonal oscillation even though the temporal negative OLR vibrations are stronger.

These analyses demonstrate that the intra-seasonal oscillation of precipitation  $\delta^{18}\text{O}$  in these regions is largely driven by the south-north direction process of the BSISO visualized on the OLR anomaly signal in Asian monsoon regions during boreal summer. The continued east-west distribution of the OLR anomaly is corresponding to the intra-seasonal oscillations of precipitation  $\delta^{18}\text{O}$  in the equatorial region.

### 3.3. The Oscillation of the Specific Convective Systems and Precipitation $\delta^{18}\text{O}$ During BSISO Propagation

Another issue is the convective activity on synoptic scales and related meteorological background conditions, which are linked to the intra-seasonal oscillation of precipitation isotopes. These specific convective systems include monsoon depressions, West Pacific tropical cyclones, Sumatra squalls, shear lines, the Meiyu-Baiu front, monsoon clusters, and so on (Figure S3 in Supporting Information S1). In this section, we will discuss the relationship among the BSISO, the activities of monsoon depressions and tropical cyclones, the vapor flux in the monsoon region, and precipitation  $\delta^{18}\text{O}$  oscillations at Nyalam and Manila. As the MD (monsoon depression) is the major contributor to the Indian summer monsoon rainfall (Yoon & Huang, 2012), and the TC (tropical cyclone) or typhoons are the most violent convective systems affecting the northwest Pacific region. We have plotted the movement paths of the MD and TC centers from May to October 2014 (Figure S2 in Supporting Information S1).

Figure 7a shows that the four MDs occurred intensively in July and three MDs occurred from late August to early September, corresponding to phases 4, 5, and 6 of the BSISO. The arrival of MD results in precipitation  $\delta^{18}\text{O}$  depletion of over  $10\text{‰}$  at Nyalam and maintains low levels during periods with frequent MDs. This result suggests that the convective phase of the BSISO leads to an increased number of MDs, which are the main precipitation systems that cause the intra-seasonal oscillation of summer precipitation  $\delta^{18}\text{O}$  in this region (Figure 7a).

There are six BSISO processes from May to October 2014 (Figure 7a). The zonal vapor flux in South Asia (South Asia uq, Figure S5 in Supporting Information S1) showed intra-seasonal oscillations during the 2nd to 5th BSISO cycle. The Southeast Asia uq represents the zonal vapor flux from the Indian Ocean to the Western Pacific Ocean and has a high correlation ( $r = 0.87$ ) with the South Asia uq. During BSISO phases 4–7 (shaded box in Figure 7a), the increasing South Asia uq represents the enhancement of vapor transport from Somalia to the Asian monsoon region, resulting in the active period of the South Asian monsoon depression and the West Pacific tropical cyclone. At the same time, the precipitation  $\delta^{18}\text{O}$  in Nyalam and Manila decreased and remained



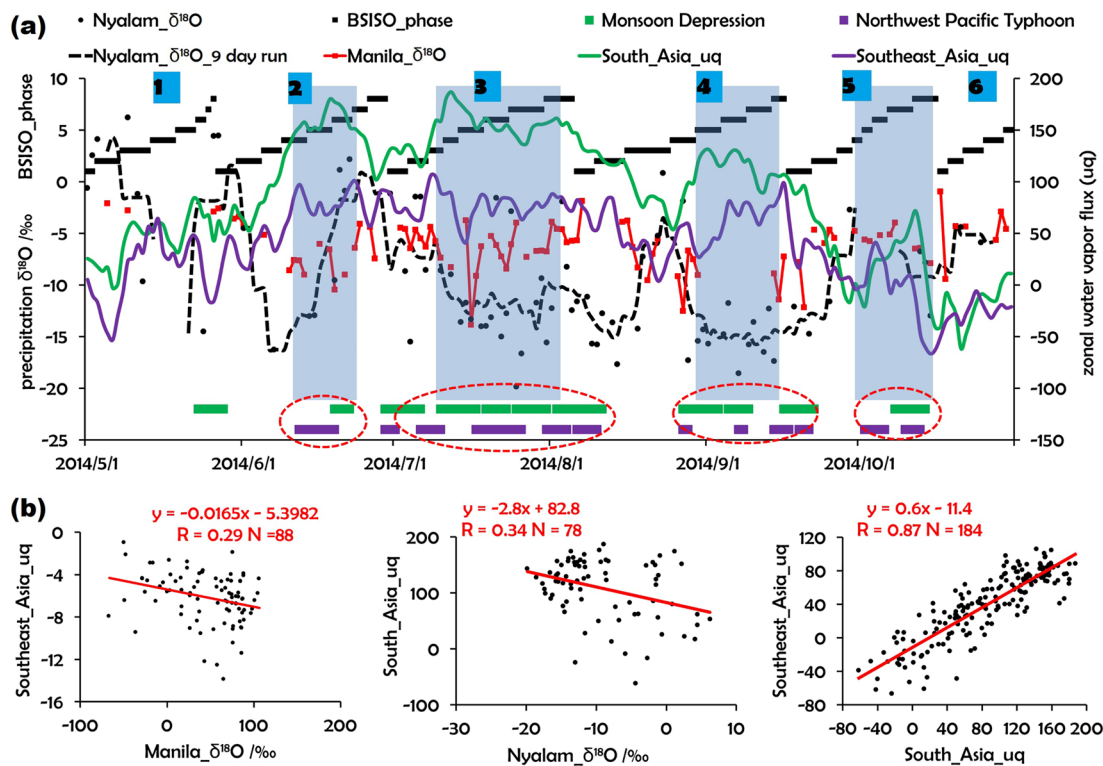


**Figure 7.** Daily variation of precipitation  $\delta^{18}\text{O}$  at Nyalam and Manila, phase of BSISO, zonal vapor flux (uq) in the region of South and Southeast Asia, and the duration of the Monsoon Depression and Northwest Pacific Typhoon (a). The marked numbers 1–6 represent the six times of the Boreal Summer Intra-seasonal Oscillation event, and the bottom oval red dashed circles represent the active periods of monsoon low pressure and typhoon. The scatter plots between Southeast Asia ( $60^\circ\text{E}$ – $90^\circ\text{E}$ ,  $5^\circ\text{N}$ – $20^\circ\text{N}$ ) uq and precipitation  $\delta^{18}\text{O}$  of Manila, between South Asia ( $105^\circ\text{E}$ – $120^\circ\text{E}$ ,  $10^\circ\text{N}$ – $20^\circ\text{N}$ ) uq and precipitation  $\delta^{18}\text{O}$  of Nyalam, between South Asia uq and Southeast Asia uq on the daily scale (b).

low. The precipitation  $\delta^{18}\text{O}$  in Manila and Nyalam is significantly correlated with the intensity of zonal monsoon vapor transport. The above results indicate that BSISO, by adjusting the meteorological background conditions, leads to the intra-seasonal oscillation of the regional convective activity and the ratio of precipitation isotopes.

## 4. Discussion

### 4.1. The Intra-Seasonal Oscillation Amplitude and Phase of Precipitation $\delta^{18}\text{O}$

The intra-seasonal oscillation of precipitation or vapor  $\delta^{18}\text{O}$  can be modulated by the BSISO or MJO (Figure S4 in Supporting Information S1), while the amplitude and phase of  $\delta^{18}\text{O}$  have spatial heterogeneity.

To address this spatial difference, we made a comprehensive comparison (Figure 8a; Table S3 in Supporting Information S1) to show the mean values ( $\mu$ ) and one standard deviation ( $1\sigma$ ) of precipitation  $\delta^{18}\text{O}$  at stations in different regions. The  $1\sigma$  values vary from  $3.3\text{‰}$  to  $4.2\text{‰}$  (mean amplitude of  $2\sigma$  from  $6.6\text{‰}$  to  $8.2\text{‰}$ ) at the equatorial station, higher than the  $1\sigma$  of Southeast and East Asian monsoon regions (with  $2.4\text{‰}$ – $3.1\text{‰}$ ). While in the South Asian region, there is a wide range of  $1\sigma$  values among different stations, varying from  $2.3\text{‰}$  to  $6.3\text{‰}$ . To study the linkage between the average precipitation  $\delta^{18}\text{O}$  and the magnitude of  $\delta^{18}\text{O}$  variations, we made a correlation analysis between one standard deviation ( $1\sigma$ ) and the mean values ( $\mu$ ) of precipitation  $\delta^{18}\text{O}$  for all stations, and the negative correlation ( $r = 0.57$ ,  $n = 18$ ,  $p < 0.05$ ) is significant (Figure 8b). This indicates more depleted precipitation  $\delta^{18}\text{O}$  is accompanied by large intra-seasonal oscillation. The underlying mechanism is analogous in that the depletion of the heavy precipitation isotope in low latitudes results from the inter-annual or seasonal variation of convective activity (Cai & Tian, 2016; Lekshmy et al., 2014). As a result, the region with stronger convective activity (the more depleted process of precipitation isotope) has stronger intra-seasonal oscillation of precipitation isotope as well.

The comparison of the amplitudes of the intra-seasonal and seasonal oscillations of precipitation  $\delta^{18}\text{O}$  at different stations in different regions is shown in Figure 8c. We found that the ratios of intra-seasonal oscillation amplitude

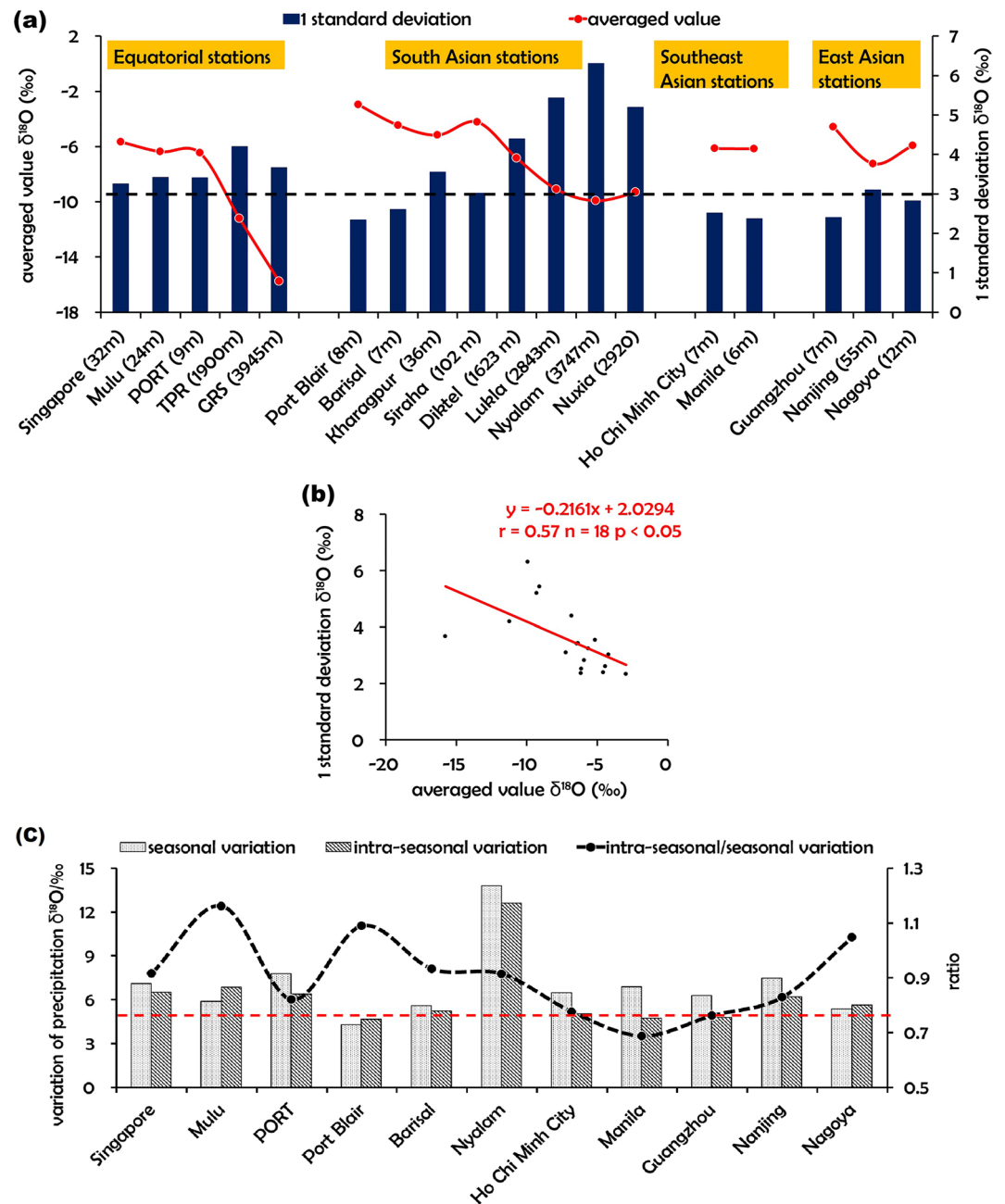


**Figure 8.** The averages and one standard deviations of precipitation  $\delta^{18}\text{O}$  in non-equatorial stations from May to October 2014, in Singapore and Mulu during the whole year of 2014, and in PORT, TPR, and GRS during 2013 and 2015 (a). The correlation scatter for one standard deviation and the average precipitation  $\delta^{18}\text{O}$  at all stations (b). The series diagram of seasonal variation, intra-seasonal variation, and the ratio between intra-seasonal variation and seasonal variation for 11 stations during 2014 (except PORT is for 2013) (c). The calculated period of intra-seasonal variation is from May to October, while for the whole year at Singapore, Mulu, and PORT. The seasonal variation is defined as the maximum value minus the minimum value on the monthly scale, and the intra-seasonal variation is defined as two times of one standard deviation.

to seasonal oscillation amplitude of precipitation  $\delta^{18}\text{O}$  at these stations vary from 0.69 to 1.16, indicating the comparable significance between the seasonal and intra-seasonal precipitation  $\delta^{18}\text{O}$  oscillation.

As precipitation itself has a strong signal of intra-seasonal oscillation, following we will discuss the relationship between the rainfall amount along the propagation of the convective cloud bands (Sengupta et al., 2020) and the intra-seasonal oscillation of precipitation isotopes. Here we selected nine stations to reveal the intra-seasonal



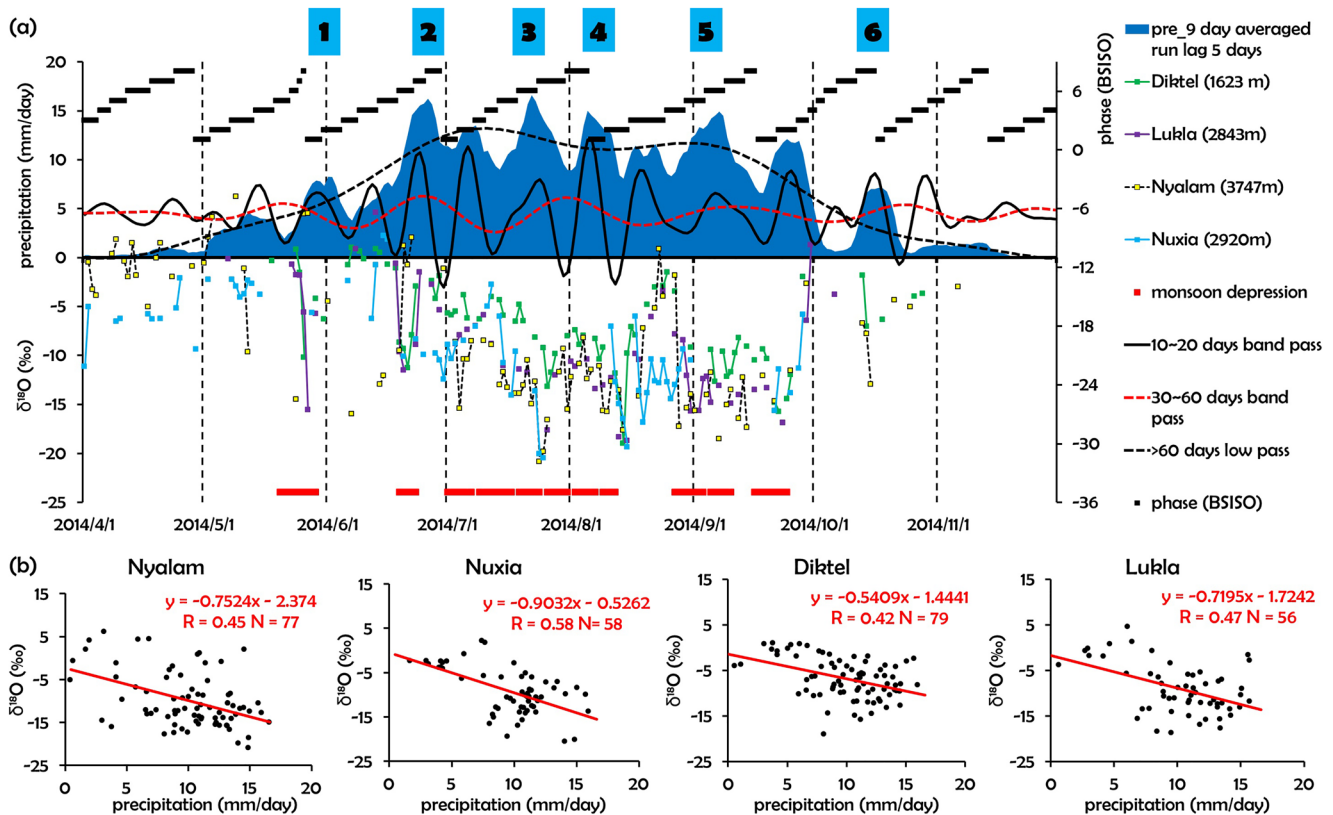


**Figure 9.** The daily precipitation  $\delta^{18}\text{O}$  of Diktel, Lukla, Nyalam, and Nuxia; the 9-day running average precipitation with a lag of 5 days (area plot in dark blue); the value after band-pass filtering of precipitation (region average value over  $80^{\circ}\text{E}$ – $95^{\circ}\text{E}$  and  $17^{\circ}\text{N}$ – $27^{\circ}\text{N}$ , red dotted box 1 in the Figure S9 in Supporting Information S1), the periods of monsoon depression and the phase of Boreal Summer Intra-seasonal Oscillation (a), the top numbers 1–6 represent the period of abundant rainfall corresponding to the period 1–6 in Figure 6a. The scatter plots between regional precipitation amount and  $\delta^{18}\text{O}$  of Diktel, Lukla, Nyalam, and Nuxia on the daily scale (b).

oscillation of average precipitation in the surrounding region and its relationship with the intra-seasonal oscillation of precipitation  $\delta^{18}\text{O}$  (Figure S9 in Supporting Information S1). The surrounding region refers to the upstream direction of ISO propagation and climatic mean vapor transport, and the meridional distance is  $10^{\circ}$ , and the horizontal distance is  $10$ – $20^{\circ}$ .

The Southern Asia stations are Nyalam, Nuxia (Figure 9), Diktel, and Lukla, and the calculated region of precipitation is shown in region 1 ( $17^{\circ}\text{N}$ – $27^{\circ}\text{N}$ ,  $80^{\circ}\text{E}$ – $95^{\circ}\text{E}$ , Figure S9 in Supporting Information S1) on the south side of the sites. We plotted the intra-seasonal oscillations of precipitation  $\delta^{18}\text{O}$  at the four stations and the 9-day running regional average precipitation amount with a lag of 5 days and conducted correlation analysis during 2014 (Figure 9b).

The regional mean precipitation in region 1 has obvious components of intra-seasonal oscillations on 10–20 days and 30–60 days, and the latter component corresponds to the BSISO. There is a significant correlation ( $P < 0.01$ ) between precipitation  $\delta^{18}\text{O}$  and regional precipitation amount at the four stations (Figure 9b). Figure 9 indicates that the BSISO produces the intra-seasonal oscillation in both precipitation amount and  $\delta^{18}\text{O}$  by regulating convective activities dominated by monsoon depression. The earlier study also found that the cumulative rainfall (during the low OLR anomaly) over the BOB has a negative correlation ( $R = -0.71$ ,  $N = 16$ ) with precipitation  $\delta^{18}\text{O}$  at Kharagpur (the northern shore of the Bay of Bengal) during 16 convective phases (Sengupta et al., 2020). Here we included both the convective and the non-convective phase, and highlight that there is a solid relationship of intra-seasonal oscillation pattern between precipitation amount and the  $\delta^{18}\text{O}$ .

We also made the correlation analysis between the regional average precipitation amount and the precipitation  $\delta^{18}\text{O}$  of the other eight stations (Figures S7–S9 in Supporting Information S1). We found that the average precipitation of the eight regions is also regulated by the intra-seasonal oscillation, and the precipitation  $\delta^{18}\text{O}$  had a significant negative correlation ( $P < 0.01$ ) with regional precipitation amount (TPR,  $R = 0.50$ ; Mulu,  $R = 0.54$ ;

Singapore,  $R = 0.45$ ; Ho Chi Minh City,  $R = 0.44$ ; Manila,  $R = 0.53$ ; Guangzhou,  $R = 0.28$ ; Nanjing,  $R = 0.41$ ; Nagoya,  $R = 0.34$ ).

#### 4.2. The Different Intra-Seasonal Oscillation Patterns Between Asian Equatorial and Monsoon Regions

In the equatorial region, the intra-seasonal oscillation is the main pattern of precipitation isotope variation, and each phase cycle of the MJO or BSISO corresponds to a fluctuation of precipitation  $\delta^{18}\text{O}$ , OLR anomaly (Figures 2 and 3), and regional precipitation amount (Figure S6 in Supporting Information S1). Also, the intra-seasonal precipitation  $\delta^{18}\text{O}$  amplitude is parallel with the amplitude of the MJO or BSISO (PCx, OLR, and the regional precipitation amount) in different seasons (Figure 3). In the northern hemisphere (Singapore and Mulu station), the intra-seasonal oscillation of precipitation  $\delta^{18}\text{O}$  can be affected by both MJO and BSISO modes and exists throughout the whole year with no obvious seasonal variation (Figure 3). While in the southern hemisphere (PORT stations), the intra-seasonal oscillation of precipitation  $\delta^{18}\text{O}$  is mainly affected by MJO mode, with weaker seasonal variation from July to October and stronger in other months (Figure 2).

The intra-seasonal oscillation of precipitation isotopes in the Asian monsoon region is much related to the seasonal precipitation pattern. In the South Asian monsoon region, the intra-seasonal oscillation of precipitation isotopes is highly consistent with the occurrence of the summer monsoon (June–September), and the BSISO of its influence mode is called MISO (Monsoon intra-seasonal oscillation) (Sengupta et al., 2020). While in Ho Chi Minh City and Manila of Southeast Asia, the intra-seasonal oscillation of precipitation isotopes can be significantly extended from June to December with the extended rainy season (Figure S7 in Supporting Information S1). In the East Asian monsoon region (Guangzhou and Nanjing), the intra-seasonal oscillation of precipitation isotopes can last from March to November (Figure S8 in Supporting Information S1). In Nagoya, the coastal station toward the northwest Pacific, the intra-seasonal oscillation of precipitation isotope can extend to the whole year with uniform seasonal precipitation (Figure S8 in Supporting Information S1).

In the Asian monsoon region, the intra-seasonal oscillation of precipitation isotopes is modulated by the BSISO or MISO during the boreal summer (Sengupta et al., 2020). The oscillation of precipitation  $\delta^{18}\text{O}$  reflects the synchronous oscillation of monsoon vapor transport intensity, regional convective system activity (Figure 7), and regional precipitation amount (Figure 10), superimposed on the seasonal and inter-annual variation. In the equatorial region, the intra-seasonal oscillation is the main pattern for the precipitation  $\delta^{18}\text{O}$  (Figure 3). These patterns are further superimposed on the inter-annual pattern of precipitation isotopes affected by the ENSO (Belgaman et al., 2016; Permana et al., 2016).

The depletion of precipitation isotopes is related to the convection process in upstream along the moisture trajectories. Therefore, we performed lag correlation analysis on precipitation  $\delta^{18}\text{O}$  between different stations (Figure 10).

With the propagation of the MJO and BSISO, there is a lag between the timing of these intra-seasonal isotope signals between different stations (Figure S4 in Supporting Information S1). The average number of days between the timing of these events can be estimated by the maximum correlation coefficient in the lag correlation analysis. These correlation analyses show that the precipitation  $\delta^{18}\text{O}$  series in Mulu is 4 days behind that in Singapore, the precipitation  $\delta^{18}\text{O}$  series in Nyalam is 5 days behind that in Barisal, and the  $\delta^{18}\text{O}$  series in Manila is 9 days later than that in Ho Chi Minh City. However, we found the lag correlation between precipitation  $\delta^{18}\text{O}$  series in East Asia is poor and is not presented here. The continuity of OLR anomaly fluctuation is stronger in South Asia (Figure 6a) and the equatorial region (Figure 6c), but weaker in East Asia (Figure 6b), which is likely the reason for the difference in precipitation  $\delta^{18}\text{O}$  lag correlation between these regions.

#### 4.3. The Intra-Seasonal Oscillation of Precipitation $\delta^{18}\text{O}$ Pattern and the Climate Implication

The ratio of stable isotope in modern precipitation is used for the interpretation and validation of climate and hydrological models, and paleoclimatic archives in tropical regions. The dominant factors influencing precipitation  $\delta^{18}\text{O}$  variation may vary from minutes (He, Goodkin, Kurita, et al., 2018) to inter-annual time scales in Asia equatorial and monsoon regions (Cai & Tian, 2016; He, Goodkin, Jackisch, et al., 2018; Lekshmy et al., 2019), making this endeavor for such a purpose in argument. The MJO plays a critical role in connecting or bridging weather and climate, involved in scale interactions across a wide range of spectrum from the

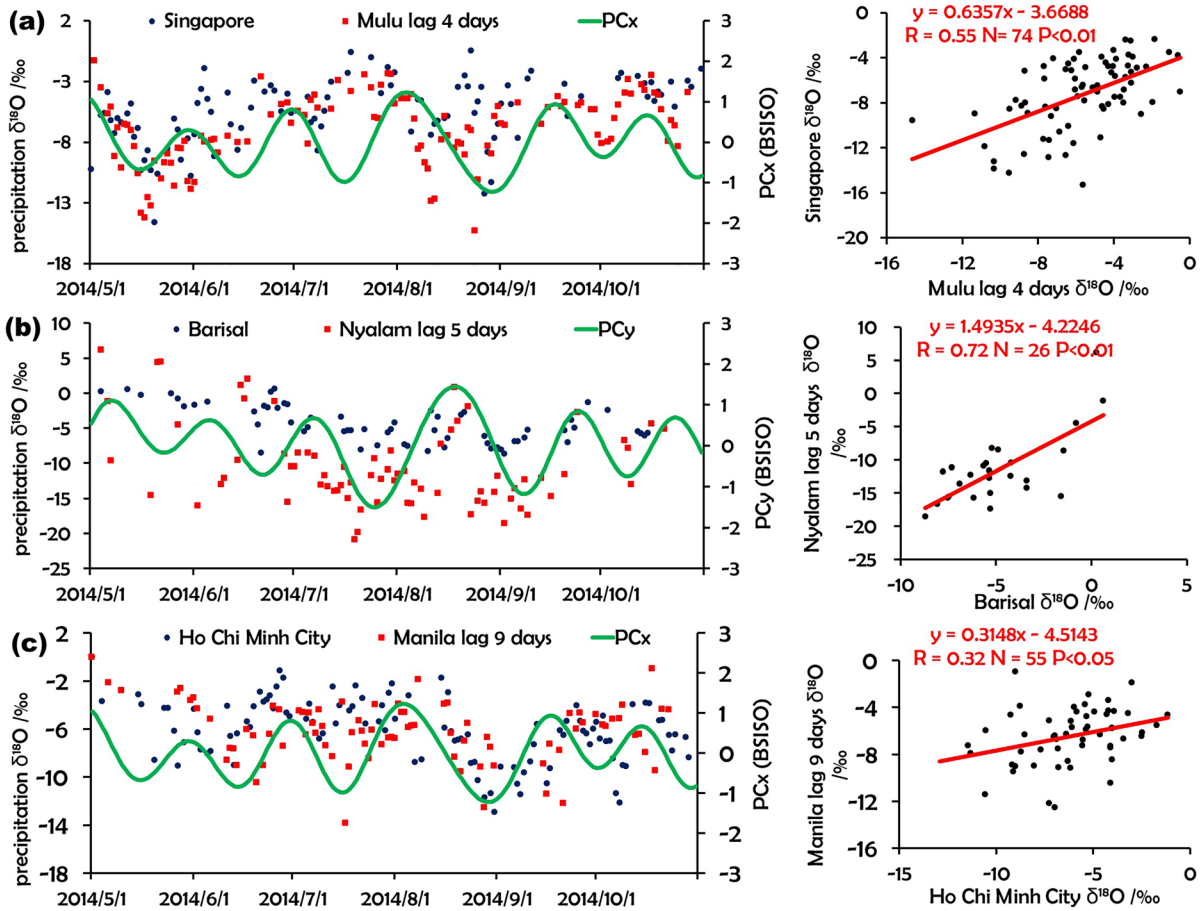


**Figure 10.** The scatter relation between two station precipitation  $\delta^{18}\text{O}$  series, but with a lag of few days: Singapore and Mulu (lag 4 days) (a), Barisal and Nyalam (lag 5 days) (b), Ho Chi Minh City and Manila (lag 9 days) (c) from May to October 2014.

diurnal cycle to the inter-annual variability (C. Zhang, 2013). The intra-seasonal oscillation of precipitation/vapor  $\delta^{18}\text{O}$  plays the similarly important role in the study of  $\delta^{18}\text{O}$  between the synoptic and the inter-seasonal time scales as well. On the synoptic scale, the low- $\delta^{18}\text{O}$  phase represented the positive anomaly of convective activity during an intra-seasonal cycle (Figure 7). On the seasonal scale, the low- $\delta^{18}\text{O}$  season corresponds to the stronger intra-seasonal oscillation of precipitation  $\delta^{18}\text{O}$  (Figures 2 and 9), and the amplitude between seasonal and intra-seasonal scales is comparable (Figure 8).

In addition, as the comprehensive performance modulated by the atmospheric intra-seasonal oscillations, the evolution of precipitation  $\delta^{18}\text{O}$  (Figure 3) can faithfully record the intensity and phase of atmospheric intra-seasonal oscillations in different regions. The MJO signal has been recorded in the proxy derived from a natural archive of giant clam shells (Yan et al., 2021). Similarly, the precipitation-related climate archives such as soil, vegetation, ice cores, stalagmites, and other sediments have the potential to rebuild the intra-seasonal oscillation signal superimposed on seasonal and inter-annual cycles. This is an additional index for the study of the MJO or BSISO yet, and it is also conducive to the study of the modern process of precipitation isotopes.

The intra-seasonal oscillation patterns of stable water isotopes are recorded in the data of vapor scanned by satellites as well. By analyzing the intra-seasonal oscillation of vapor  $\delta\text{D}$  from IASI, the pattern of vapor  $\delta\text{D}$  on the global scale can be identified. The distributions of negative vapor  $\delta\text{D}$  anomaly appear at 2,950, 4,220, and 6,380 m a. s. l. above the Eastern Indian Ocean and Indonesian Archipelago during the spring of 2015 with the convective phase of MJO (Figure S10 in Supporting Information S1). The vapor  $\delta\text{D}$  in the convective phase is 40‰ to 90‰ lower than in the non-convective phase. The activity of MJO leads to the east-west contrast pattern for vapor  $\delta\text{D}$  between the convective active and inactive regions from the equatorial Indian Ocean to the Pacific Ocean in our results, which is also found in the study of TES data (Hurley et al., 2019).

## 5. Conclusions

In this study, we discussed the intra-seasonal oscillation pattern of precipitation or vapor  $\delta^{18}\text{O}$  covering the Asian monsoon and equatorial regions. We found different behavior of the intra-seasonal response in precipitation and/or vapor  $\delta^{18}\text{O}$  in both the lasting months and varying magnitude between the two regions.

The stations in the southern equator are mainly affected by the MJO modes, and the precipitation  $\delta^{18}\text{O}$  has obvious intra-seasonal oscillations from December to May, and the dilution period of precipitation  $\delta^{18}\text{O}$  corresponds to phases 4, 5, and 6 of the MJO, with average amplitude from 6.2‰ to 7.8‰. The stations in the northern equator can be affected by both the MJO (DJFMA) and the BSISO (JJASO) modes, and the precipitation  $\delta^{18}\text{O}$  has intra-seasonal oscillations throughout the year with average amplitude from 6.2‰ to 7‰. The dilution precipitation  $\delta^{18}\text{O}$  periods are at phases 2, 3, 4, and 5 of the ISO.

In the Asian monsoon stations, the precipitation  $\delta^{18}\text{O}$  has a significant intra-seasonal oscillation pattern during the rainy season with average amplitudes ranging from 4.6‰ to 12.6‰. In the convective phase of BSISO, the region influenced by the dilution precipitation  $\delta^{18}\text{O}$  moves northward with the northward transmission of the convective zone. During phases 4, 5, and 6 of BSISO, more monsoon depression and tropical cyclone events appear in the South Asia monsoon region and Southwest Pacific Ocean, respectively, with more monsoon zonal vapor flux, leading to the dilution phase of precipitation  $\delta^{18}\text{O}$  within the intra-seasonal oscillation pattern in Asian monsoon regions.

The intra-seasonal oscillation amplitude of precipitation  $\delta^{18}\text{O}$  had an obvious negative correlation with the average precipitation  $\delta^{18}\text{O}$  covering the stations. This indicated that the intra-seasonal oscillation of precipitation  $\delta^{18}\text{O}$  was stronger in regions with stronger convective activity. Moreover, the intra-seasonal oscillation of precipitation  $\delta^{18}\text{O}$  can correspond to the intra-seasonal oscillation of precipitation amount in the upstream region. Except for the East Asian monsoon region, the precipitation  $\delta^{18}\text{O}$  has significant lag correlation between the stations in the direction of ISO propagation, which may be related to the propagation of continuous OLR anomaly belt in these regions.

## Data Availability Statement

The precipitation  $\delta^{18}\text{O}$  data for Nyalam can retrieve from the Supporting Information S1 file (Table S5) of this article. The precipitation  $\delta^{18}\text{O}$  data for Nuxia and Guangzhou are downloaded from the National Tibetan Plateau Data Center, China (<http://data.tpdc.ac.cn/zh-hans>) (X. Yang, Davis, et al., 2018). The vapor  $\delta^{18}\text{O}$  data for Qianyanzhou (27m AGL) is from the Stable Water Vapor Isotope Database, Yale University (<https://vapor-isotope.yale.edu>). The  $\delta^{18}\text{O}$  data for Siraha, Diktel, and Lukla from the supplementary file of Acharya et al. (2020), (<https://doi.org/10.1016/j.quaint.2020.09.052>). The  $\delta^{18}\text{O}$  data for PORT (Port site), TPR (Tembagapura), and GRS (Grasberg) are from the Byrd Polar and Climate Research Center, Ohio State University (<https://byrd.osu.edu/research/groups/ice-core-paleoclimatology/data>) (Permana et al., 2016). The  $\delta^{18}\text{O}$  data for Barisal, Port Blair, Nagoya, Mulu, Singapore, and Ho Chi Minh City are from the database of the IAEA's Coordinated Research Project (CRP) F31004 (<https://figshare.com/s/dfdabb43a844cad530a5>) (Munksgaard et al., 2019). The  $\delta^{18}\text{O}$  data of Manila, Kharagpur, and Nanjing are from the data share of earlier literature (<https://nhess.copernicus.org/articles/22/213/2022/nhess-22-213-2022-supplement.pdf>, <https://link.springer.com/article/10.1007/s00382-020-05344-w#additional-information>, and <https://data.tpdc.ac.cn/en/data/d117f51c-b47f-4bfd-9030-0c54f15067cf/>) (Jackisch et al., 2022; Y. Li et al., 2020; Sengupta et al., 2020; Xu et al., 2021). Except for the data periods of PORT, TPR, and GRS, which are for 2013 and 2015, the data of other stations are for 2014. The interpolated outgoing longwave radiation (OLR) data (Liebmann & Smith, 1996) are from the Physical Sciences Laboratory of NOAA (<https://psl.noaa.gov/data/gridded/data.olrcdr.interp.html>). The daily reanalysis climate data ( $u$  wind,  $v$  wind, and specific humidity) are from ERA5 (<https://cds.climate.copernicus.eu/cdsapp#!/dataset/reanalysis-era5-pressure-levels?tab=form>), with a spatial resolution of  $0.25^\circ \times 0.25^\circ$ . The phases and indexes  $\text{PC}_x$  or  $\text{PC}_y$  of BSISO and MJO are from the International Climate Research Center ([http://iprc.soest.hawaii.edu/users/kazuyosh/Bimodal\\_ISO.html](http://iprc.soest.hawaii.edu/users/kazuyosh/Bimodal_ISO.html)). The typhoon track and intensity data for the northwest Pacific Ocean are from the website of Typhoon Online (<https://www.typhoon.org.cn/>). The regional precipitation data are from the GPCP (<https://www.ncei.noaa.gov/products/global-precipitation-climatology-project>). The satellite data of  $\delta\text{D}$  from the global and multi-annual MUSICA IASI  $\{\text{H}_2\text{O}, \delta\text{D}\}$  pair data set ([https://radar.kit.edu/radar/en/dataset/eIgWmcoTbvouxnm. Regular%2B1%25C2%25B0x1%25C2%25B0%2Bre-gridded%2BMUSICA%](https://radar.kit.edu/radar/en/dataset/eIgWmcoTbvouxnm. Regular%2B1%25C2%25B0x1%25C2%25B0%2Bre-gridded%2BMUSICA%2)



2BIAS%2Bwater%2Bisotopologue%2Bpair%2Bdataset%2B%2528a%2Bposteriori%2Bprocessing%2Bversion%2B%2529#) (Diekmann et al., 2021).

### Acknowledgments

This study is supported by the National Natural Science Foundation of China (U2202208), the Strategic Priority Research Program of the Chinese Academy of Sciences (XDB40000000), and the Science and Technology Department of Yunnan Province (202201BF070001-021). We sincerely thank the three anonymous reviewers for their constructive comments and suggestions, which have improved the quality of the manuscript.

### References

- Acharya, S., Yang, X., Yao, T., & Shrestha, D. (2020). Stable isotopes of precipitation in Nepal Himalaya highlight the topographic influence on moisture transport. *Quaternary International*, *565*, 22–30. <https://doi.org/10.1016/j.quaint.2020.09.052>
- Andersen, K. K., Azuma, N., Barnola, J.-M., Bigler, M., Biscaye, P., Caillon, N., et al. (2004). High-resolution record of Northern Hemisphere climate extending into the last interglacial period. *Nature*, *431*(7005), 147–151. <https://doi.org/10.1038/nature02805>
- Araguás-Araguás, L., Froehlich, K., & Rozanski, K. (1998). Stable isotope composition of precipitation over southeast Asia. *Journal of Geophysical Research*, *103*(D22), 28721–28742. <https://doi.org/10.1029/98JD02582>
- Belgaman, H. A., Ichiyanagi, K., Tanoue, M., & Suwarman, R. (2016). Observational research on stable isotopes in precipitation over Indonesian maritime continent. *Journal of Japanese Association of Hydrological Sciences*, *46*(1), 7–28. <https://doi.org/10.4145/jahs.46.7>
- Brown, J., Simmonds, I., & Noone, D. (2006). Modeling  $\delta^{18}\text{O}$  in tropical precipitation and the surface ocean for present-day climate. *Journal of Geophysical Research*, *111*(D5), D05105. <https://doi.org/10.1029/2004JD005611>
- Cai, Z., & Tian, L. (2016). Atmospheric controls on seasonal and interannual variations in the precipitation isotope in the East Asian monsoon region. *Journal of Climate*, *29*(4), 1339–1352. <https://doi.org/10.1175/JCLI-D-15-0363.1>
- Cai, Z., Tian, L., & Bowen, G. J. (2017). ENSO variability reflected in precipitation oxygen isotopes across the Asian Summer Monsoon region. *Earth and Planetary Science Letters*, *475*, 25–33. <https://doi.org/10.1016/j.epsl.2017.06.035>
- Cai, Z., Tian, L., & Bowen, G. J. (2018). Spatial-seasonal patterns reveal large-scale atmospheric controls on Asian Monsoon precipitation water isotope ratios. *Earth and Planetary Science Letters*, *503*, 158–169. <https://doi.org/10.1016/j.epsl.2018.09.028>
- Chakraborty, S., Sinha, N., Chattopadhyay, R., Sengupta, S., Mohan, P. M., & Datye, A. (2016). Atmospheric controls on the precipitation isotopes over the Andaman Islands, Bay of Bengal. *Scientific Reports*, *6*(1), 19555. <https://doi.org/10.1038/srep19555>
- Cheng, H., Zhang, H., Zhao, J., Li, H., Ning, Y., & Kathayat, G. (2019). Chinese stalagmite paleoclimate researches: A review and perspective. *Science China Earth Sciences*, *62*(10), 1489–1513. <https://doi.org/10.1007/s11430-019-9478-3>
- Dansgaard, W. (1964). Stable isotopes in precipitation. *Tellus*, *16*(4), 436–468. <https://doi.org/10.3402/tellus.v16i4.8993>
- Diekmann, C. J., Schneider, M., Ertl, B., Hase, F., García, O., Khosravi, F., et al. (2021). The global and multi-annual MUSICA IASI ( $\text{H}_2\text{O}$ ,  $\delta\text{D}$ ) pair dataset [Dataset]. *Earth System Science Data*, *13*(11), 5273–5292. <https://doi.org/10.5194/essd-13-5273-2021>
- Donald, A., Meinke, H., Power, B., Maia, A. d. H. N., Wheeler, M. C., White, N., et al. (2006). Near-global impact of the Madden-Julian Oscillation on rainfall. *Geophysical Research Letters*, *33*(9), L09704. <https://doi.org/10.1029/2005GL025155>
- Dong, W., Lin, Y., Wright, J. S., Ming, Y., Xie, Y., Wang, B., et al. (2016). Summer rainfall over the southwestern Tibetan Plateau controlled by deep convection over the Indian subcontinent. *Nature Communications*, *7*(1), 10925. <https://doi.org/10.1038/ncomms10925>
- Goswami, B. N. (1987). A mechanism for the west-north-west movement of monsoon depressions. *Nature*, *326*(6111), 376–378. <https://doi.org/10.1038/326376a0>
- Goswami, B. N., Ajayamohan, R. S., Xavier, P. K., & Sengupta, D. (2003). Clustering of synoptic activity by Indian summer monsoon intraseasonal oscillations. *Geophysical Research Letters*, *30*(8). <https://doi.org/10.1029/2002GL016734>
- Goswami, B. N., & Mohan, R. S. A. (2001). Intraseasonal oscillations and interannual variability of the Indian summer monsoon. *Journal of Climate*, *14*(6), 1180–1198. [https://doi.org/10.1175/1520-0442\(2001\)014<1180:IOAIVO>2.0.CO;2](https://doi.org/10.1175/1520-0442(2001)014<1180:IOAIVO>2.0.CO;2)
- He, S., Goodkin, N. F., Jackisch, D., Ong, M. R., & Samanta, D. (2018). Continuous real-time analysis of the isotopic composition of precipitation during tropical rain events: Insights into tropical convection. *Hydrological Processes*, *32*(11), 1531–1545. <https://doi.org/10.1002/hyp.11520>
- He, S., Goodkin, N. F., Kurita, N., Wang, X., & Rubin, C. M. (2018). Stable isotopes of precipitation during tropical Sumatra Squalls in Singapore. *Journal of Geophysical Research: Atmospheres*, *123*(7), 3812–3829. <https://doi.org/10.1002/2017JD027829>
- Hurley, J. V., Verlinden, K. L., Blossley, P. N., Kuang, Z., & Noone, D. (2019). Moist entropy and water isotopologues in a zonal overturning circulation framework of the Madden-Julian Oscillation. *Journal of Geophysical Research: Atmospheres*, *124*(3), 1248–1265. <https://doi.org/10.1029/2018JD029510>
- Islam, M., Rahman, M., Gebrekirstos, A., & Bräuning, A. (2021). Tree-ring  $\delta^{18}\text{O}$  climate signals vary among tree functional types in South Asian tropical moist forests. *Science of The Total Environment*, *756*, 143939. <https://doi.org/10.1016/j.scitotenv.2020.143939>
- Jackisch, D., Yeo, B. X., Switzer, A. D., He, S., Cantarero, D. L. M., Siringan, F. P., & Goodkin, N. F. (2022). Precipitation stable isotopic signatures of tropical cyclones in Metropolitan Manila, Philippines, show significant negative isotopic excursions. *Natural Hazards and Earth System Sciences*, *22*(1), 213–226. <https://doi.org/10.5194/nhess-22-213-2022>
- Jiang, X., Adames, Á. F., Kim, D., Maloney, E. D., Lin, H., Kim, H., et al. (2020). Fifty years of research on the Madden-Julian Oscillation: Recent progress, challenges, and perspectives. *Journal of Geophysical Research: Atmospheres*, *125*(17), e2019JD030911. <https://doi.org/10.1029/2019JD030911>
- Kikuchi, K. (2021). The boreal summer intraseasonal oscillation (BSISO): A review. *Journal of the Meteorological Society of Japan*, *99*(4), 933–972. <https://doi.org/10.2151/jmsj.2021-045>
- Kikuchi, K., Wang, B., & Kajikawa, Y. (2012). Bimodal representation of the tropical intraseasonal oscillation. *Climate Dynamics*, *38*(9), 1989–2000. <https://doi.org/10.1007/s00382-011-1159-1>
- Kurita, N., Fujiyoshi, Y., Nakayama, T., Matsumi, Y., & Kitagawa, H. (2015). East Asian Monsoon controls on the inter-annual variability in precipitation isotope ratio in Japan. *Climate of the Past*, *11*(2), 339–353. <https://doi.org/10.5194/cp-11-339-2015>
- Kurita, N., Noone, D., Risi, C., Schmidt, G. A., Yamada, H., & Yoneyama, K. (2011). Intraseasonal isotopic variation associated with the Madden-Julian Oscillation. *Journal of Geophysical Research*, *116*(D24). <https://doi.org/10.1029/2010JD015209>
- Lekshmy, P. R., Midhun, M., & Ramesh, R. (2019). Amount dependency of monsoon rainfall  $\delta^{18}\text{O}$  on multiple time scales: Observations from southwestern India. *Climate Dynamics*, *53*(1), 933–941. <https://doi.org/10.1007/s00382-019-04620-8>
- Lekshmy, P. R., Midhun, M., Ramesh, R., & Jani, R. A. (2014).  $^{18}\text{O}$  depletion in monsoon rain relates to large scale organized convection rather than the amount of rainfall. *Scientific Reports*, *4*(1), 5661. <https://doi.org/10.1038/srep05661>
- Li, T. (2014). Recent advance in understanding the dynamics of the Madden-Julian oscillation. *Journal of Meteorological Research*, *28*(1), 1–33. <https://doi.org/10.1007/s13351-014-3087-6>
- Li, Y., An, W., Pang, H., Wu, S.-Y., Tang, Y., Zhang, W., & Hou, S. (2020). Variations of stable isotopic composition in atmospheric water vapor and their controlling factors—A 6-year continuous sampling study in Nanjing, eastern China. *Journal of Geophysical Research: Atmospheres*, *125*(22), e2019JD031697. <https://doi.org/10.1029/2019JD031697>



- Liebmann, B., & Smith, C. (1996). Description of a complete (interpolated) outgoing longwave radiation dataset. *Bull. Amer. Meteor. Soc.*, 77, 1275–1277.
- Liu, Y., Cobb, K. M., Song, H., Li, Q., Li, C. Y., Nakatsuka, T., et al. (2017). Recent enhancement of central Pacific El Niño variability relative to last eight centuries. *Nature Communications*, 8(1), 15386. <https://doi.org/10.1038/ncomms15386>
- Madden, R. A., & Julian, P. R. (1972). Description of global-scale circulation cells in the tropics with a 40–50 day period. *Journal of the Atmospheric Sciences*, 29(6), 1109–1123. [https://doi.org/10.1175/1520-0469\(1972\)029<1109:DOGSCC>2.0.CO;2](https://doi.org/10.1175/1520-0469(1972)029<1109:DOGSCC>2.0.CO;2)
- Midhun, M., Lekshmy, P. R., & Ramesh, R. (2013). Hydrogen and oxygen isotopic compositions of water vapor over the Bay of Bengal during monsoon. *Geophysical Research Letters*, 40(23), 6324–6328. <https://doi.org/10.1002/2013GL058181>
- Midhun, M., Lekshmy, P. R., Ramesh, R., Yoshimura, K., Sandeep, K. K., Kumar, S., et al. (2018). The Effect of monsoon circulation on the stable isotopic composition of rainfall. *Journal of Geophysical Research: Atmospheres*, 123(10), 5205–5221. <https://doi.org/10.1029/2017JD027427>
- Moerman, J. W., Cobb, K. M., Adkins, J. F., Sodemann, H., Clark, B., & Tuen, A. A. (2013). Diurnal to interannual rainfall  $\delta^{18}\text{O}$  variations in northern Borneo driven by regional hydrology. *Earth and Planetary Science Letters*, 369–370, 108–119. <https://doi.org/10.1016/j.epsl.2013.03.014>
- Munksgaard, N. C., Kurita, N., Sánchez-Murillo, R., Ahmed, N., Araguas, L., Balachew, D. L., et al. (2019). Data Descriptor: Daily observations of stable isotope ratios of rainfall in the tropics [Dataset]. *Scientific Reports*, 9(1), 14419. <https://doi.org/10.1038/s41598-019-50973-9>
- Murgulet, V., & Aharon, P. (2008). Stalagmite  $\delta^{18}\text{O}$  variability records of ENSO-Controlled rainfall from Niue Island, South Pacific. In *AGU fall meeting abstracts*.
- Pang, H., Hou, S., Zhang, W., Wu, S., Jenk, T. M., Schwikowski, M., & Jouzel, J. (2020). Temperature trends in the northwestern Tibetan Plateau constrained by ice core water isotopes over the past 7,000 Years. *Journal of Geophysical Research: Atmospheres*, 125(19), e2020JD032560. <https://doi.org/10.1029/2020JD032560>
- Permana, D. S., Thompson, L. G., & Setyadi, G. (2016). Tropical West Pacific moisture dynamics and climate controls on rainfall isotopic ratios in southern Papua, Indonesia. *Journal of Geophysical Research: Atmospheres*, 121(5), 2222–2245. <https://doi.org/10.1002/2015JD023893>
- Porter, S. E., Mosley-Thompson, E., Thompson, L. G., & Wilson, A. B. (2021). Reconstructing an Interdecadal Pacific Oscillation index from a Pacific Basin-wide collection of ice core records. *Journal of Climate*, 34(10), 1–43. <https://doi.org/10.1175/jcli-d-20-0455.1>
- Rahul, P., Ghosh, P., Bhattacharya, S. K., & Yoshimura, K. (2016). Controlling factors of rainwater and water vapor isotopes at Bangalore, India: Constraints from observations in 2013 Indian monsoon. *J Geophys Res-Atmos*, 121(23), 13936–13952. <https://doi.org/10.1002/2016jd025352>
- Ramesh, R., Bhattacharya, S. K., & Pant, G. B. (1989). Climatic significance of  $\delta\text{D}$  variations in a tropical tree species from India. *Nature*, 337(6203), 149–150. <https://doi.org/10.1038/337149a0>
- Risi, C., Bony, S., Vimeux, F., Descroix, L., Ibrahim, B., Lebreton, E., et al. (2008). What controls the isotopic composition of the African monsoon precipitation? Insights from event-based precipitation collected during the 2006 AMMA field campaign. *Geophysical Research Letters*, 35(24), L24808. <https://doi.org/10.1029/2008GL035920>
- Sengupta, S., Bhattacharya, S. K., Parekh, A., Nimya, S. S., Yoshimura, K., & Sarkar, A. (2020). Signatures of monsoon intra-seasonal oscillation and stratiform process in rain isotope variability in northern Bay of Bengal and their simulation by isotope enabled general circulation model. *Climate Dynamics*, 55(5), 1649–1663. <https://doi.org/10.1007/s00382-020-05344-w>
- Shao, L. L., Tian, L., Cai, Z. Y., Cui, J. P., Zhu, D., Chen, Y. H., & Palcsu, L. (2017). Driver of the interannual variations of isotope in ice core from the middle of Tibetan Plateau. *Atmospheric Research*, 188, 48–54. <https://doi.org/10.1016/j.atmosres.2017.01.006>
- Sinha, A., Kathayat, G., Cheng, H., Breitenbach, S. F. M., Berkelhammer, M., Mudelsee, M., et al. (2015). Trends and oscillations in the Indian summer monsoon rainfall over the last two millennia. *Nature Communications*, 6(1), 6309. <https://doi.org/10.1038/ncomms7309>
- Sperber, K. R., Slingo, J. M., & Annamalai, H. (2000). Predictability and the relationship between subseasonal and interannual variability during the Asian summer monsoon. *Quarterly Journal of the Royal Meteorological Society*, 126(568), 2545–2574. <https://doi.org/10.1002/qj.49712656810>
- Tan, L., Shen, C. C., Löwemark, L., Chawchai, S., Edwards, R. L., Cai, Y., et al. (2019). Rainfall variations in central Indo-Pacific over the past 2,700 y. *Proceedings of the National Academy of Sciences*, 116(35), 17201–17206. <https://doi.org/10.1073/pnas.1903167116>
- Thompson, L. G., Yao, T., Davis, M. E., Henderson, K. A., Mosley-Thompson, E., Lin, P. N., et al. (1997). Tropical climate instability: The last glacial cycle from a Qinghai-Tibetan ice core. *Science*, 276(5320), 1821–1825. <https://doi.org/10.1126/science.276.5320.1821>
- Thompson, L. G., Yao, T., Mosley-Thompson, E., Davis, M. E., Henderson, K. A., & Lin, P. N. (2000). A high-resolution millennial record of the South Asian monsoon from Himalayan ice cores. *Science*, 289(5486), 1916–1919. <https://doi.org/10.1126/science.289.5486.1916>
- Vimeux, F., Gallaire, R., Bony, S., Hoffmann, G., & Chiang, J. C. H. (2005). What are the climate controls on  $\delta\text{D}$  in precipitation in the Zongo Valley (Bolivia)? Implications for the Illimani ice core interpretation. *Earth and Planetary Science Letters*, 240(2), 205–220. <https://doi.org/10.1016/j.epsl.2005.09.031>
- Vuille, M., & Werner, M. (2005). Stable isotopes in precipitation recording South American summer monsoon and ENSO variability: Observations and model results. *Climate Dynamics*, 25(4), 401–413. <https://doi.org/10.1007/s00382-005-0049-9>
- Wang, D., Tian, L. D., Cai, Z. Y., Shao, L. L., Guo, X. Y., Tian, R., et al. (2020). Indian monsoon precipitation isotopes linked with high level cloud cover at local and regional scales. *Earth and Planetary Science Letters*, 529, 115837. <https://doi.org/10.1016/j.epsl.2019.115837>
- Wang, S., Ma, D., Sobel, A. H., & Tippett, M. K. (2018). Propagation characteristics of BSISO indices. *Geophysical Research Letters*, 45(18), 9934–9943. <https://doi.org/10.1029/2018GL078321>
- Wheeler, M. C., & Hendon, H. H. (2004). An all-season real-time multivariate MJO Index: Development of an index for monitoring and prediction. *Monthly Weather Review*, 132(8), 1917–1932. [https://doi.org/10.1175/1520-0493\(2004\)132<1917:AARMMI>2.0.CO;2](https://doi.org/10.1175/1520-0493(2004)132<1917:AARMMI>2.0.CO;2)
- Xu, T., Pang, H., Zhan, Z.-W., Zhang, W., Guo, H., Wu, S., & Hou, S. (2021). Water vapor isotopes indicating rapid shift among multiple moisture sources for the 2018/2019 winter extreme precipitation events in Southeast China. *Hydrology and Earth System Sciences Discussions*, 26, 117–127. <https://doi.org/10.5194/hess-26-117-2022>
- Yan, H., Zhao, N., Zhou, P., Liu, C., Fei, H., Li, M., et al. (2021). The first detection of the Madden-Julian Oscillation signal in daily to hourly resolution proxy records derived from a natural archive of Giant Clam Shell (*Tridacna* spp.). *Earth and Planetary Science Letters*, 555, 116703. <https://doi.org/10.1016/j.epsl.2020.116703>
- Yang, H., Johnson, K. R., Griffiths, M. L., & Yoshimura, K. (2016). Interannual controls on oxygen isotope variability in Asian monsoon precipitation and implications for paleoclimate reconstructions. *Journal of Geophysical Research: Atmospheres*, 121(14), 8410–8428. <https://doi.org/10.1002/2015jd024683>
- Yang, X., Davis, M. E., Acharya, S., & Yao, T. (2018). Asian monsoon variations revealed from stable isotopes in precipitation. *Climate Dynamics*, 51(5), 2267–2283. <https://doi.org/10.1007/s00382-017-4011-4>
- Yang, X., Yao, T., Deji, Zhao, H., & Xu, B. (2018). Possible ENSO influences on the northwestern Tibetan Plateau revealed by annually resolved ice core records. *Journal of Geophysical Research: Atmospheres*, 123(8), 3857–3870. <https://doi.org/10.1002/2017JD027755>
- Yang, X., Yao, T., Yang, W., Xu, B., He, Y., & Qu, D. (2012). Isotopic signal of earlier summer monsoon onset in the Bay of Bengal. *Journal of Climate*, 25(7), 2509–2516. <https://doi.org/10.1175/JCLI-D-11-00180.1>

- Yoon, J.-H., & Huang, W.-R. (2012). Indian monsoon depression: Climatology and variability. <https://doi.org/10.5772/37917>
- Zhang, C. (2005). Madden-Julian Oscillation. *Reviews of Geophysics*, 43(2). <https://doi.org/10.1029/2004RG000158>
- Zhang, C. (2013). Madden-Julian Oscillation: Bridging weather and climate. *Bulletin of the American Meteorological Society*, 94(12), 1849–1870. <https://doi.org/10.1175/BAMS-D-12-00026.1>
- Zhang, H., Cheng, H., Spötl, C., Cai, Y., Sinha, A., Tan, L., et al. (2018). A 200-year annually laminated stalagmite record of precipitation seasonality in southeastern China and its linkages to ENSO and PDO. *Scientific Reports*, 8(1), 12344. <https://doi.org/10.1038/s41598-018-30112-6>
- Zwart, C., Munksgaard, N. C., Kurita, N., & Bird, M. I. (2016). Stable isotopic signature of Australian monsoon controlled by regional convection. *Quaternary Science Reviews*, 151, 228–235. <https://doi.org/10.1016/j.quascirev.2016.09.010>